Development 140, 126-135 (2013) doi:10.1242/dev.082701


# Rho signalling restriction by the RhoGAP *Stard13* integrates growth and morphogenesis in the pancreas

**Kristin M. Petzold, Heike Naumann and Francesca M. Spagnoli***

## SUMMARY

The development of functional organ architecture relies on coordinated morphogenesis and growth. In the developing pancreas, the branching epithelium is organised in discrete domains, delineating one specific domain of progenitor cells at the tip of the branches. The molecular mechanisms underlying the coordinated action of branching and proliferation in organ formation are largely unknown. Here, we identify the RhoGAP protein Stard13 as an essential regulator of pancreas tissue architecture in the mammalian embryo. Conditional ablation of *Stard13* expression in the pancreas disrupts epithelial morphogenesis and tip-domain organisation, resulting in hampered proliferation of tip progenitors and subsequent organ hypoplasia. *Stard13* acts by regulating Rho signalling spatially and temporally during pancreas development. Our findings provide new insights into the mechanisms that shape pancreatic epithelium to create a mature organ and establish a functional link between Rho-mediated control of epithelial remodelling and organ size determination, involving reciprocal interaction of actin-MAL/SRF and MAPK signalling pathways.

**KEY WORDS: Epithelial morphogenesis, MAPK/ERK, Pancreas development, Rho-GTPases, RhoGAP, Mouse**

## INTRODUCTION

Coordination of tissue growth and morphogenesis is crucial for generating adult functional organs (Hogan and Kolodziej, 2002; Lu and Werb, 2008). How the two processes are integrated during the development of many organs is still a major unresolved question. During pancreatic development, branching morphogenesis coincides with growth and differentiation (Jensen, 2004; Pan and Wright, 2011; Puri and Hebrok, 2010; Spagnoli, 2007). As different pancreatic cell types become specified, they organise themselves into discrete domains along the axis of the branches, delineating, for instance, a multipotent progenitor cell domain at the distal tips of the branching epithelium (Zhou et al., 2007). Importantly, recent observations have shown that the initial number of these progenitors pre-determines the final pancreas organ size (Stanger et al., 2007). Thus, establishment of a proper progenitor pool size during branching phase [between embryonic stage (E)12 and E14 in the mouse embryo] is crucial for normal pancreas formation and function, including digestion and blood sugar regulation. However, the molecular mechanisms underlying the coordinated action of branching and progenitor proliferation in the developing pancreas are largely unknown.

Small Rho GTPases play a fundamental role in the control of morphogenesis and cell proliferation of several epithelial organs (Van Aelst and Symons, 2002; Etienne-Manneville and Hall, 2002; Kesavan et al., 2009). GTPases act as molecular switches, cycling between active GTP-bound and inactive GDP-bound states, a process that is tightly regulated by distinct classes of proteins, including the Rho GTPases-activating proteins (GAPs) (Tcherkezian and Lamarche-Vane, 2007). Specifically, GAPs inactivate GTPases by accelerating their intrinsic GTPase activity thereby converting them into the inactive GDP-bound form (Sordella et al., 2003; Tcherkezian and Lamarche-Vane, 2007). Because of the ubiquitous distribution of small GTPases, a restricted expression of GAPs appears to be fundamental for the precise spatial-temporal regulation of their activity.

Here, we have identified the RhoGAP Stard13 [also called Shirin in *Xenopus* embryos (Spagnoli and Brivanlou, 2006) and deleted liver cancer (DLC) 2 in humans (Leung et al., 2005)], as a tissue-specific GTPase regulator of mammalian pancreas development. Genetic ablation of *Stard13* disrupts epithelial branching and distal tip-domain morphogenesis, resulting in hampered proliferation of pancreatic progenitors and subsequent organ hypoplasia. We show that Stard13 acts by regulating Rho signalling spatially and temporally during pancreas development. Finally, our results suggest a reciprocal interaction between the Rho-actin and mitogen-activated protein kinase (MAPK) signalling pathways to regulate progenitor cell proliferation locally. Together, these results identify Stard13 as a molecular integrator of growth and morphogenesis that acts by restricting Rho-actin activity in the pancreas.

## MATERIALS AND METHODS

### Mouse strains

A gene-targeting vector for creating a floxed allele of the mouse *Stard13* gene was generated using bacterial homologous recombination. The standard two-loxP site strategy was adapted to the use of bacterial artificial chromosomes (BACs) as targeting vectors (Valenzuela et al., 2003). The BAC-containing *Escherichia coli* carrying the entire *Stard13* gene locus (BAC clone RP23-11K10) was identified by the alignment of BAC end sequences in the NCBI database. Chimeric mice were generated by injection of four independently targeted embryonic stem (ES) cells into blastocysts, and the allele was passed through the germline. The $Stard13^{flox(Hygro)/+}$ mice were crossed to a germline *Flp-deleter* mouse strain (Rodriguez et al., 2000) to remove the Hygro cassette. Removal of the Hygro cassette was confirmed by PCR and Southern blot (data not shown). Further information on the targeting vector, targeting of ES cells, generation of $Stard13^{flox}$ mice and genotyping can be found in supplementary material Fig. S1. $Stard13^{flox/flox}$ mice were interbred with CMV-Cre mice (Schwenk et al., 1995) to generate mice carrying a germline-deleted allele of *Stard13* ($Stard13^{\Delta}$; supplementary material Fig. S1) and with *Pdx1-Cre* transgenic mice for conditional ablation in the pancreas (Gu et al., 2002). All animal

Laboratory of Molecular and Cellular Basis of Embryonic Development, Max Delbrück Center for Molecular Medicine, Robert-Rössle-Strasse 10, D-13125 Berlin, Germany.

*Author for correspondence (francesca.spagnoli@mdc-berlin.de)

**Accepted 16 October 2012**

experimentation was conducted in accordance with the local ethics committee for animal care.

#### Reverse transcription and quantitative PCR

For RNA isolation, embryonic tissues were dissected and snap-frozen on dry ice. Subsequently, RNA was extracted with RNAzol (Biozol) according to manufacturer's instructions and total RNA was used for reverse transcription using random hexamers and oligodT and the SuperScript III First-Strand Synthesis System (Invitrogen) according to instructions. Real-time PCR reactions were carried out using the SYBR Green Master Mix (Roche) on ABI StepOne Plus system. Succinate dehydrogenase (SDHA) and ribosomal protein 36B4 were used as reference genes. All the values were normalised to the reference genes and calculated using the software REST (Pfaffl et al., 2002). Data were determined in triplets. See supplementary material Table S1 for primer sequences.

#### Immunohistochemistry and *in situ* hybridisation

Mouse embryos and pancreata were fixed in 4% paraformaldehyde at 4°C from 2 hours to overnight. Subsequently, samples were equilibrated in 20% sucrose solution and embedded in OCT compound (Sakura). *In situ* hybridisation on cryostat sections was carried out as described by Schaeren-Wiemers and Gerfin-Moser (Schaeren-Wiemers and Gerfin-Moser, 1993). Cryosections (10 μm) were incubated with TSA (Perkin Elmer) blocking buffer for 1 hour at room temperature and afterwards with primary antibodies at the appropriate dilution (supplementary material Table S2). Immunostainings were analysed with Zeiss AxioObserver, Zeiss LSM 700 and LeicaSPE laser scanning microscopes. For counting, pancreatic tissue of at least three wild-type (WT) and three Stard13$^{PA\text{-}deleted}$ embryos were cut into serial sections and stained cells were counted on every third sections. E-cadherin (cadherin 1)$^{+}$ pancreatic epithelium was measured using AxioVision software (Zeiss). Quantification of immunohistochemical markers focused on the dorsal pancreas. Quantification of the fluorescence intensity of the F-actin staining was measured using ImageJ software on confocal images. The ROI tool was used to measure the Integrated Density values (sum of the values of the pixels in the selection) in Pdx1$^{+}$ area of 5-10 optical sections from a minimum of three different experiments. For morphometric analyses, E18.5 pancreata were fixed in 4% paraformaldehyde and paraffin embedded. Each pancreas was sectioned at three different levels and for each level three sections (4 μm) were collected on a slide. Total pancreatic area identified was quantified using a Scan Scope microscope, analysed by Image Scope viewer (Aperio Technologies, USA) and expressed in μm$^2$. The average cell surface was determined on at least five pancreata for each genotype. All results are expressed as mean±s.e.m. and significance of differences between groups was evaluated with Student's *t*-test.

#### Transmission electron microscopy

E12.5 pancreata were fixed in phosphate-buffered 2.5% glutaraldehyde for 4 hours at 4°C and postfixed in 1% $OsO_4$. Samples were dehydrated and embedded in epoxy resin. Thin sections were counterstained with uranil acetate and lead citrate and examined with a Hitachi H-7100FA microscope.

#### Pancreatic explants

Dorsal pancreatic buds were microdissected from mouse embryos at E11.5 and cultured on glass-bottom dishes (Matek) pre-coated with 50 μg/ml sterile bovine fibronectin (Invitrogen) in Basal Medium Eagle (BME) supplemented with 10% foetal bovine serum (Horb and Slack, 2000; Petzold and Spagnoli, 2012). Cultures were maintained for up to 6 days at 37°C in 5% $CO_2$. The day of plating is referred to as day 0. For the Rho inhibition assay, membrane-permeable C3 transferase (Cytoskeleton) was added at a final concentration of 2.5 μg/ml to the culture medium on day 1 and replaced every 24 hours. The Rho/SRF pathway inhibitor CCG-1423 (Millipore) was added at the final concentration of 5 μM to the culture medium on day 1 and replaced every 24 hours. In the extracellular signal-regulated kinase (ERK) inhibition assay, PD0325901 (Selleck) was added at a final concentration of 2 μM. Explants were fixed in 4% paraformaldehyde, stained as whole-mounts and analysed using a Zeiss LSM 700 confocal laser scanning microscope. For phospho-histone H3 (pHH3) counting, the E-cadherin$^{+}$ volume of pancreatic explants of at least three WT and three *Stard13*$^{PA\text{-}deleted}$ embryos was measured on acquired confocal *z*-stacks using Huygens software (Scientific Volume Imaging).

#### Pull-down assay

For Rho-GTP pull-down assay, dissected E17.5 pancreata were snap frozen in liquid nitrogen. After genotyping, pancreata were lysed and ~300 μg total protein extract was incubated with 25 μg Rhotekin-RDB beads according to manufacturer's instructions (Cytoskeleton). One-tenth of the total lysate (~25-30 μg) was used for total Rho western blot. Immunoblots were incubated with anti-Rho antibody (1:500; Cytoskeleton) and analysed using the LI-COR Odyssey system.

#### Glucose tolerance test

Glucose tolerance test was carried out on three-month-old male animals that had been fasting overnight, before the day of experimentation (time point –1). Animals were injected intraperitoneally with glucose (2 g/kg body weight). Glucose levels were measured from blood collected from the tail immediately before the glucose challenge (time point 0) and 15, 30, 60 and 120 minutes after the glucose injection using a blood glucose meter (Contour, Bayer).

#### Statistical tests

All results are expressed as mean ± s.e.m. The significance of differences between groups was evaluated with Student's *t*-test. $P<0.05$ was considered statistically significant.

## RESULTS

### Stard13 controls proliferation of pancreatic progenitor cells

*In situ* hybridisation analysis revealed an early expression of *Stard13* in the developing pancreas from E10.5 onwards in the mouse embryo (Fig. 1A). Notably, at the onset of branching, *Stard13* showed a regionalised expression pattern, being enriched at the distal tips of the epithelial branches (Fig. 1A), which are known to contain multipotent progenitors capable of generating all pancreatic cell types (Horb and Slack, 2000; Zhou et al., 2007).

To examine whether *Stard13* regulates pancreas morphogenesis and tip-domain organisation, we generated a conditional *Stard13* (*Stard13*$^{flox}$) mutant allele (supplementary material Fig. S1) and intercrossed these mice with *Pdx1-cre* transgenic mice for conditional gene ablation in all pancreatic cell types during embryonic development (Gu et al., 2002). In wild-type (WT) pancreas, branching morphogenesis started normally and well-formed primary branches were visible from E12.5 onwards (Fig. 1B). By contrast, in *Stard13*$^{flox/flox}$; *Pdx1-Cre* [from here on referred to as *Stard13*$^{PA\text{-}deleted}$ (*Stard13*-pancreas deleted)] embryos, the pancreatic tissue failed to form branching structures, displaying a globular shape with internal cavities, though pancreatic fate was normally specified, as judged by Pdx1 expression (Fig. 1B). Because the *Stard13* transcript was enriched at the distal tips of the branching epithelium, we investigated whether its ablation affects the typical tip-domain organisation of the pancreatic epithelium (Zhou et al., 2007). To this aim, we analysed the expression of carboxypeptidase A1 (Cpa1), which is confined to WT tip domains and marks tip progenitor cells between E12.5 and E14.5 (Zhou et al., 2007) (Fig. 1B). Cpa1$^{+}$ cells were also detected in *Stard13*$^{PA\text{-}deleted}$ pancreas, but they displayed random distribution throughout the tissue, and tip structures were not properly formed (Fig. 1B). Subsequently, at E16.5, mature pancreatic tubular networks and acinar structures were evident in the WT, whereas *Stard13*$^{PA\text{-}deleted}$ ducts and acini appeared as malformed large cellular aggregates (Fig. 1B). These results indicate that Stard13 controls morphogenesis and establishment of proper tip domain within the pancreatic branches during embryonic development.

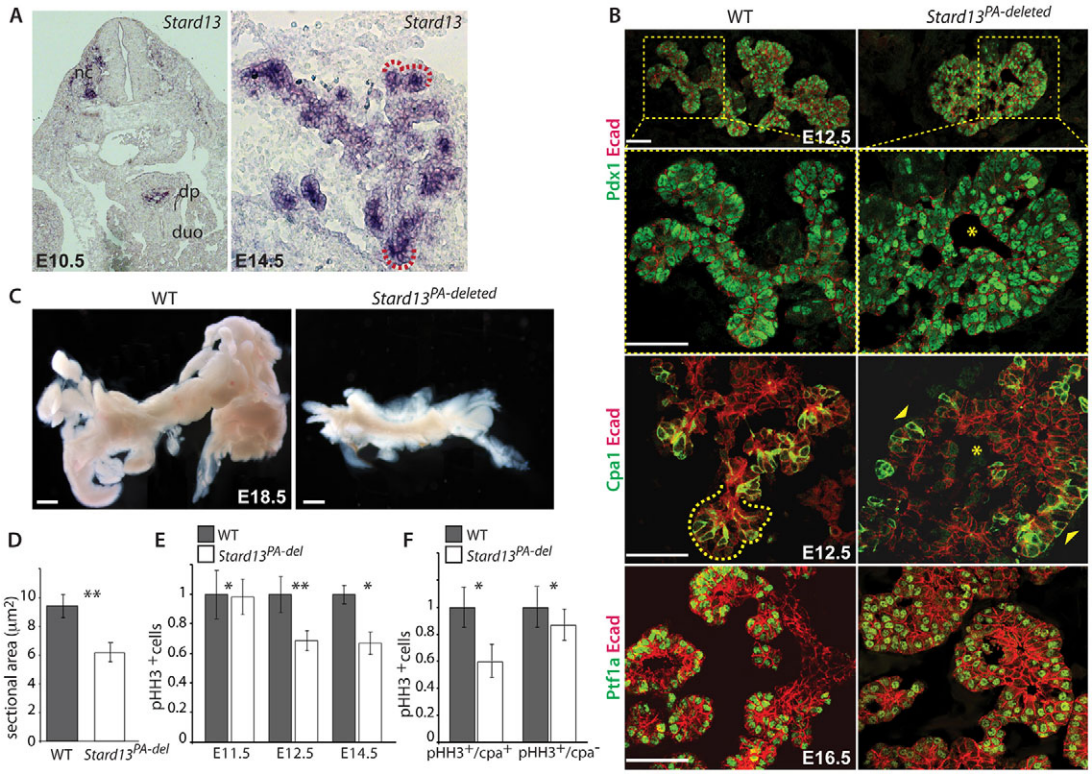


**Fig. 1. Stard13 controls pancreatic branching morphogenesis.** (**A**) *In situ* hybridisation analysis for *Stard13* on cryosections of mouse embryos. *Stard13* transcript accumulates at the tip of epithelial branches (red outline). No expression of *Stard13* is detected in the mesenchyme surrounding the pancreatic epithelium. dp, dorsal pancreatic bud; duo, duodenum; nc, neural crest territory. (**B**) Immunofluorescence analysis of Pdx1, E-cadherin (Ecad), Cpa1 and Ptf1a (Kawaguchi et al., 2002) in WT and *Stard13*$^{PA\text{-}deleted}$ pancreas. Cpa1$^{+}$ cells are confined to the distal tip cells of WT pancreatic branches (yellow dotted outline), but are scattered throughout the epithelium in *Stard13*$^{PA\text{-}deleted}$ pancreas (arrowheads). Asterisks indicate internal cavities. (**C**) *Stard13* ablation results in pancreas hypoplasia, which is visible by gross morphological examination at E18.5. (**D**) Morphometric analysis of pancreas surface area in WT and *Stard13*$^{PA\text{-}deleted}$ pancreata at E18.5. *Stard13*$^{PA\text{-}deleted}$ newborns exhibit smaller mean sectional area of pancreata than that of WT littermates (sectional area *Stard13*$^{PA\text{-}deleted}$=6.16±0.66, *n*=5; sectional area WT=9.41±0.83, *n*=6). (**E**) Relative number of pHH3$^{+}$ cells versus total area of the pancreatic epithelium (Ecad$^{+}$) shows reduction of proliferating cells in E12.5 *Stard13*$^{PA\text{-}deleted}$ pancreas. *n*=5. A similar decrease in pancreatic cell proliferation persisted at E14.5. (**F**) *Stard13*$^{PA\text{-}deleted}$ epithelium shows reduced numbers of pHH3$^{+}$Cpa1$^{+}$ cells at E12.5 compared with WT. *n*=4. All results are expressed as mean ± s.e.m. **P*<0.05, ***P*<0.01, determined by Student's *t*-test. Scale bars: in B, 50 µm; in C, 1 mm.

In the pancreas, organ growth relies on proliferation of progenitor cells and coincides with the time of branching morphogenesis (Seymour et al., 2007; Stanger et al., 2007). Indeed, at the onset of branching, between E11.5 and E12.5, proliferation rate undergoes a 20-fold increase in the WT pancreas epithelium (our unpublished data). We therefore examined whether aberrant morphogenesis in *Stard13*$^{PA\text{-}deleted}$ embryonic pancreas affects pancreas growth. Gross examination of neonatal pancreata revealed severe pancreatic hypoplasia in *Stard13*$^{PA\text{-}deleted}$ mice, which was also assessed by morphometry (Fig. 1C,D; supplementary material Fig. S1). Postnatally, *Stard13*$^{PA\text{-}deleted}$ animals were growth retarded and displayed impaired glucose tolerance (supplementary material Fig. S2). We found that *Stard13* was expressed not only throughout pancreatic development but also in the endocrine islets after birth (Fig. 1; data not shown). We performed a glucose tolerance test (GTT) on WT and mutant animals of same age. Although basal blood glucose levels appeared normal, the curve was characterised by a slower and delayed return to basal levels after the glucose challenges in *Stard13*$^{PA\text{-}deleted}$ animals. These results suggest a role for the RhoGAP Stard13 in β-cell function during adulthood.

We then explored whether alterations in cell proliferation and/or apoptosis during embryogenesis are responsible for pancreatic size reduction in *Stard13*$^{PA\text{-}deleted}$ mice. Very few apoptotic cells were detected within normal pancreatic epithelium during embryonic stages E12.5-16.5 and apoptosis was not increased in the pancreas of *Stard13*$^{PA\text{-}deleted}$ embryos, as determined by TUNEL assay and caspase 3 immunostaining (data not shown). By contrast, immunohistochemical measurements of proliferation using the mitosis-specific marker phospho-histone H3 (pHH3) revealed a 27% average decrease in cell proliferation in *Stard13*$^{PA\text{-}deleted}$ E12.5 pancreas compared with WT (Fig. 1E). Importantly, reduced cell proliferation was observed at E12.5 in the mutant pancreas compared with WT, whereas there was no difference between mutant and WT pancreas at E11.5 (Fig. 1E).

To examine whether *Stard13* ablation specifically affects proliferation of progenitor cells, we analysed the percentage of proliferating cells that express the progenitor marker Cpa1. In the *Stard13*$^{PA\text{-}deleted}$ pancreatic epithelium, a strong reduction in the number of pHH3$^{+}$Cpa1$^{+}$ pancreatic cells was observed (40% reduction; Fig. 1F), whereas the percentage of pHH3$^{+}$Cpa1$^{-}$ cells was similar between WT and mutant pancreata (only 13% reduction; Fig. 1F). Similar results were obtained upon bromodeoxyuridine (BrdU) *in vivo* labelling at E12.5 and quantification of double BrdU$^{+}$Cpa1$^{+}$ cells (data not shown). These measurements indicated that the 27% proliferation reduction is mainly due to reduced cell proliferation of the Cpa1$^{+}$ cell compartment (Fig. 1F). Consistent with

their decreased proliferative activity, Cpa1$^+$ cells were reduced in *Stard13*$^{PA\text{-}deleted}$ embryos at later stages (supplementary material Fig. S3J). Moreover, we found that ablation of *Stard13* did not affect specification of any pancreatic cell type in particular and that the relative numbers of differentiated cell types (e.g. endocrine and exocrine cells between E12.5 and E16.5) were similar in both WT and *Stard13*$^{PA\text{-}deleted}$ embryos (supplementary material Fig. S3), ruling out the possibility of accelerated differentiation of progenitor cells. Thus, our finding indicates that *Stard13* ablation hampers proliferation of pancreatic cells and, in particular, the Cpa1$^+$ progenitor pool at early embryonic stages, ultimately resulting in organ hypoplasia. Moreover, these results suggest that Stard13 control on morphogenesis is required to maintain proliferating Cpa1$^+$ cells at the branching stage and allows their expansion.

## *Stard13* is required for epithelial remodelling of the developing pancreas

We next sought to gain insight into the cellular defects at the origin of altered pancreas morphogenesis in the absence of the RhoGAP Stard13. Branching morphogenesis involves the restructuring of the pancreatic epithelium into a complex and highly organised tubular network, starting with the transition from a non-polarised cell mass to polarised epithelial monolayers between E11.5 and E12.5 in the mouse embryo (Hick et al., 2009; Jensen, 2004; Kesavan et al., 2009; Villasenor et al., 2010). We examined cell morphology and epithelial polarity, including cell-cell and cell-extracellular matrix (ECM) adhesions, and cytoskeleton organisation. In E12.5 WT pancreas, epithelial cells displayed a columnar polarised shape with basal nuclei and constricted apical pole and were radially oriented around common lumens to form branched tubular structures (Fig. 2A-C). Polarised cells showed E-cadherin confined to the basolateral membrane, F-actin, mucin 1 and atypical protein kinase C (aPKC) isoform ζ at the apical surface, and laminin and integrins at the basal lamina (Fig. 2A,B; Fig. 5; supplementary material Fig. S4). Notably, the *Stard13*$^{PA\text{-}deleted}$ epithelium did not undergo similar epithelial remodelling: the epithelium stayed stratified, displaying cells cuboidal in shape that were arranged in a disorderly fashion and randomly oriented to surround microlumens (Fig. 2A-C). Ultrastructural analysis corroborated the clear differences in epithelial organisation between WT and *Stard13*$^{PA\text{-}deleted}$ epithelia (Fig. 2C). Moreover, quantitative measurement of cell outlines defined an increased circularity index in the mutant compared with WT (Fig. 2D), which is consistent with absence or delay of cell-shape change (from cuboidal to columnar) in *Stard13*$^{PA\text{-}deleted}$ epithelium. Mutant epithelial cells characterised by a pronounced rounded shape were evident already at E11.5 (Fig. 2D).

Laminin and integrins (α3-, α6- and β1-integrins) exhibited unchanged levels and normal basal distribution in the *Stard13*$^{PA\text{-}deleted}$ epithelium relative to WT (Fig. 2A; Fig. 5). By contrast, we found that the major cytoskeletal components, such as F-actin and myosin (activated phospho-myosin II), not only accumulated to high levels but also were irregularly distributed throughout the cytoplasm in mutant cells (Fig. 2B,E). Polarised distribution of the actomyosin network normally forms cable-like structures that span multiple cells and their coordinated apical contraction results in multicellular structures, which are named rosettes in various epithelial tissues undergoing morphogenesis (Zallen and Blankenship, 2008). Upon closer analysis of E11.5 and E12.5 WT pancreas epithelium, we detected similar multicellular 'rosette-like' aggregates that displayed asymmetric enrichment of F-actin and phospho-myosin II on the apical side and that constricted their shared interfaces to form microlumens (Fig. 2E). By contrast, *Stard13*$^{PA\text{-}deleted}$ epithelial cells occasionally clustered together at a common interface, lacking localised actomyosin distribution and coordinated apical constriction (Fig. 2E). Consequently, fewer higher-order rosettes were formed and did not properly resolve (Fig. 2E).

Collectively, these results suggest alterations in actomyosin cytoskeletal organisation as the source of defective pancreatic epithelium remodelling, including defects in cell-shape changes, cell arrangement and microlumen connection, in *Stard13* mutants.

## Stard13 acts by regulating Rho signalling in the developing pancreas

Although Stard13 has been shown to have GAP activity for RhoA *in vitro* (Leung et al., 2005), its activity *in vivo* has remained unknown. To elucidate the molecular mechanism of Stard13 function, we tested whether it regulates Rho and whether its ablation leads to elevated levels of active Rho in the developing pancreas. We performed two independent assays that are based on the use of the Rho-binding domain of the Rho effector protein rhotekin fused to glutathione-s-transferase (RDB-GST) as substrate (Malliri et al., 2002). Notably, these assays are designed to detect specifically the Rho proteins in their active GTP-bound conformation and not merely their expression. First, active GTP-bound Rho was detected by RDB-GST pull-down assay in *Stard13*$^{PA\text{-}deleted}$ embryonic pancreas, whereas no detectable amounts were found in WT pancreas (Fig. 3A). Second, to visualise GTP-bound Rho proteins we used an immunolocalisation assay (Cascone et al., 2003) on cultures of E11.5 pancreas (Fig. 3C) (Horb and Slack, 2000; Petzold and Spagnoli, 2012; Puri and Hebrok, 2007). Indeed, cultured WT pancreas explants recapitulated *in vivo* early pancreatic morphogenetic and differentiation events, providing a valuable *ex vivo* model to analyse branching and tubulogenesis (Hick et al., 2009; Horb and Slack, 2000; Kesavan et al., 2009) (Fig. 3B; supplementary material Fig. S5). Strikingly, *Stard13*$^{PA\text{-}deleted}$ pancreatic explants cultured in the same conditions as WT displayed smaller size and failed to form branching structures, reproducing *ex vivo* the phenotype observed *in vivo* in the mutant pancreas (Fig. 1; Fig. 3B), and showed clusters of cells exhibiting active Rho (Fig. 3C). Taken together, these results indicate that the RhoGAP Stard13 is required to restrain the levels of active Rho in the developing pancreas.

Because ablation of *Stard13* resulted in noticeable active Rho in the pancreas, we reasoned that constraining Rho activity might rescue tissue architecture in *Stard13*$^{PA\text{-}deleted}$ pancreas. To address this possibility, we took advantage of the established pancreatic explant culture system and performed pharmacological inhibition of Rho signalling using a membrane-permeable version of the enzyme C3 ribosyltransferase (hereafter termed C3), which inactivates all Rho proteins, but not Cdc42 or Rac (Bishop and Hall, 2000). Upon exposure to C3, *Stard13*$^{PA\text{-}deleted}$ pancreatic explants started to form tubular aggregates that branched and expanded in overall size compared with untreated *Stard13*$^{PA\text{-}deleted}$ explants (Fig. 3D), implying that specific Rho inhibition is able to rescue both epithelial and proliferation defects, to some extent. In line with this, we also observed that treatment of WT pancreatic explants with lysophosphatidic acid (LPA), an activator of endogenous Rho (Malliri et al., 2002), led to rudimentary aggregates, which mimicked the *Stard13*$^{PA\text{-}deleted}$ phenotype (Fig. 4; supplementary material Fig. S5).

In the absence of *Stard13*, we found accumulation of and altered distribution of F-actin and activated myosin II *in vivo* (Fig. 2B,E) as well as *ex vivo* in pancreatic explants (Fig. 4A). F-actin content started to increase at E11.5 and progressively accumulated over

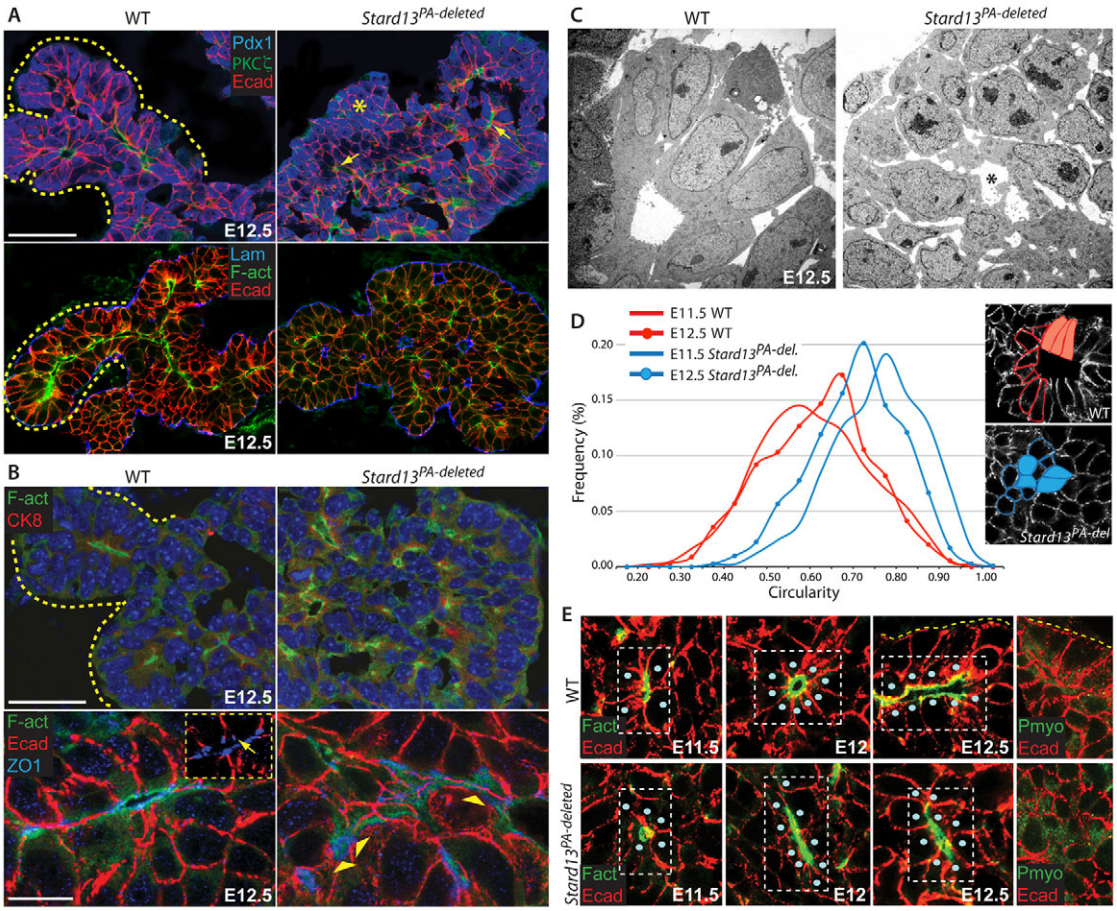


**Fig. 2. Cytoskeletal organisation defects in *Stard13*$^{PA\text{-}deleted}$ pancreatic epithelium.** (**A**) Immunostaining analysis for aPKCζ, F-actin (F-act), laminin (Lam) and Ecad shows global differences in tissue organisation between WT and *Stard13*$^{PA\text{-}deleted}$ E12.5 pancreatic epithelia. *Stard13*$^{PA\text{-}deleted}$ cells display stratified and compact epithelial organisation (asterisks). Arrows indicate cells clustered to form disorganised 'rosette-like' structures in *Stard13*$^{PA\text{-}deleted}$ epithelium. (**B**) Immunostaining of F-act, cytokeratin 8 (CK8; also known as Krt8) and tight junction-specific protein zonula occludens (ZO)-1 (also known as Tjp1) in E12.5 pancreatic epithelium. *Stard13*$^{PA\text{-}deleted}$ epithelial cells display abnormal accumulation of F-act (see arrowheads). Discrete distribution of ZO-1 at the boundary between apical and lateral domains was seen in WT cells facing lumens (see arrow in magnified inset), whereas it was irregularly accumulated in clusters in the mutant (arrowheads). Yellow dotted outlines indicate branches in A and B. (**C**) Ultrastructural analysis by transmission electron microscopy (TEM) shows WT pancreatic epithelium composed of tall cylindrical cells radially oriented around a common lumen, whereas *Stard13*$^{PA\text{-}deleted}$ cells are cuboidal and randomly oriented (asterisk). (**D**) Frequency distribution of cell circularity in E11.5 and E12.5 WT and *Stard13*$^{PA\text{-}deleted}$ epithelia. Circularity values were assigned to cell outlines using the ImageJ circularity plugin (http://rsb.info.nih.gov/ij/plugins/circularity.html) where circularity = $4\pi(\text{area}/\text{perimeter}^2)$. Circularity was measured in at least 500 cells per genotype and embryonic stage. Images on the right show examples of cell shape observed in WT and *Stard13*$^{PA\text{-}deleted}$ epithelia. (**E**) Dynamics of multicellular aggregate ('rosette-like' structures; circumscribed by white boxed areas) formation in WT and *Stard13*$^{PA\text{-}deleted}$ pancreatic epithelia between E11.5 and E12.5. F-act and phospho-Myosin II (Pmyo) are enriched at the apical pole of WT cells in forming rosettes (E11.5), in high-order vertices (E12) and in resolving rosettes (E12.5). In *Stard13*$^{PA\text{-}deleted}$ cells, Pmyo is abnormally distributed. Circles indicate the centre of each cell in the rosette-like structures. Scale bars: in A,B (upper panels), 50 μm; in B (bottom panels), 10 μm. TEM magnification, 4000× (C).

time, as judged by fluorescence intensity measurements (Fig. 4B). To address whether uninhibited Rho activity is responsible for the aberrant actomyosin network in *Stard13*$^{PA\text{-}deleted}$ epithelium, we examined F-actin distribution in explant cultures that were treated with C3. Importantly, reduction of active Rho levels in C3-treated *Stard13* mutant pancreas organ cultures not only rescued branching morphogenesis but also restored asymmetric F-actin distribution at the apical cell surface (Fig. 4A) and F-actin levels to near those of WT (Fig. 4C). By contrast, in mutant and LPA-treated WT explants F-actin fluorescence intensity increased and its distinct apical distribution was lost, being detectable all around the cell periphery, similar to the *Stard13* mutant *in vivo* phenotype (Fig. 2; Fig. 4A-C). Accumulation and aberrant F-actin network distribution are consistent with the abnormal apical width and rounded cell shape of the mutant epithelial cells (Kuure et al., 2010) (Fig. 2). Taken together, these findings indicate that *Stard13* controls epithelial remodelling and morphogenesis by regulating the Rho/actin signalling axis within the pancreatic epithelium.

## Integration of the Rho-actin and MAPK signalling pathways locally regulates progenitor cell proliferation

In branching morphogenesis, surrounding mesenchymal cues are known to play a crucial role in promoting cell proliferation in the epithelium and guiding the direction of the outgrowth (Hogan and Kolodziej, 2002; Horb and Slack, 2000; Lu and Werb, 2008;

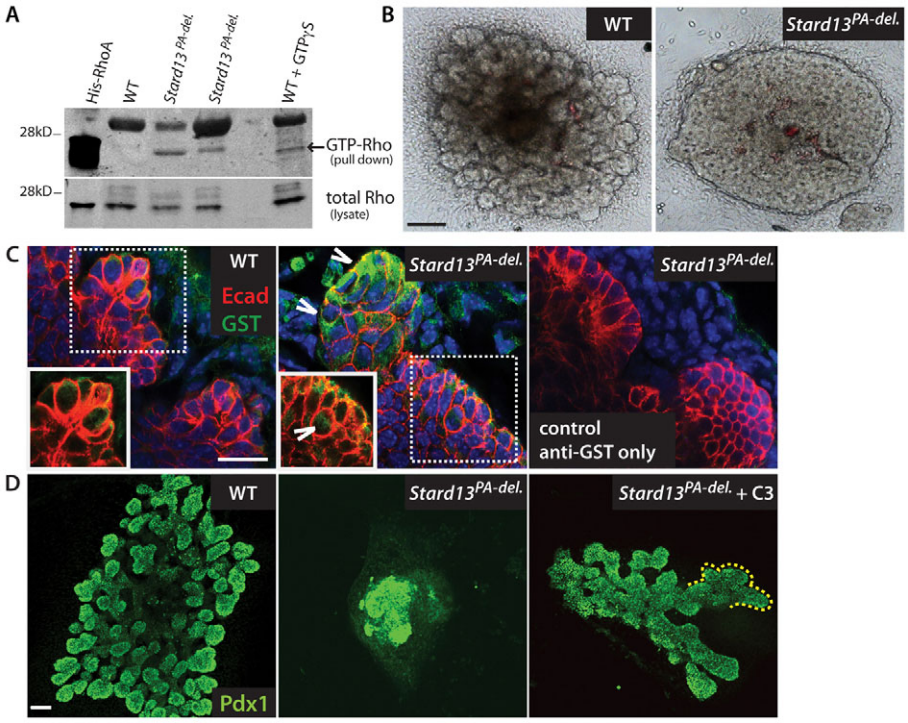


**Fig. 3. *Stard13* negatively regulates Rho activity in the developing pancreas.** (**A**) GST-RDB pull down performed on pancreatic lysates of WT and two distinct *Stard13*$^{PA\text{-}deleted}$ embryos. Pull-down (GTP-Rho; arrow) and total lysates were immunoblotted with anti-Rho antibody. WT lysate pre-loaded with the non-hydrolysable GTP analogue GTPγS (WT+GTPγS) (Cascone et al., 2003) and His-tagged RhoA fusion protein were used as positive controls in the assay. The band present above Rho is caused by non-specific binding to the RDB-GST-beads. (**B**) WT and *Stard13*$^{PA\text{-}deleted}$ pancreas organ cultures, dissected at E11.5 and cultured for 3 days. (**C**) Immunolocalisation assay with GST-RDB on pancreatic organ cultures. WT and *Stard13*$^{PA\text{-}deleted}$ pancreatic explants were incubated with RDB-GST purified protein and subsequently processed for immunofluorescence with anti-GST antibody (Cascone et al., 2003). Open arrowheads indicate localisation of active Rho-GTP bound (GST; green) in Ecad$^{+}$ pancreatic cells (red) in *Stard13*$^{PA\text{-}deleted}$ embryos. As negative controls, pancreatic explants were incubated with anti-GST antibody alone. Blue, Hoechst nuclear counterstain. Insets show area within dotted box without nuclear counterstain. (**D**) Specific Rho inhibition rescues tip morphogenesis in *Stard13*$^{PA\text{-}deleted}$ pancreatic explants. E11.5 WT, untreated *Stard13*$^{PA\text{-}deleted}$ and *Stard13*$^{PA\text{-}deleted}$ C3 transferase-treated pancreatic explants cultured for 4 days, fixed and whole-mount immunostained for Pdx1. Yellow outline marks rescued branches in C3-treated *Stard13*$^{PA\text{-}deleted}$ explants. Scale bars: in B,C 50 μm; in D, 100 μm.

Metzger et al., 2008; Watanabe and Costantini, 2004). Once pancreatic tip domains are formed, they possibly require a special supporting 'environment' for fast-proliferating progenitors to expand. Previous studies have shown that MAPK signalling factors, such as epidermal growth factor (EGF) and fibroblast growth factor (FGF) molecules, are crucial mediators of epithelial-mesenchymal interaction during pancreatic development (Bhushan et al., 2001; Edlund, 2002). In order to determine whether MAPK signalling might play a role in sustaining pancreatic local proliferation, for example at the branch tips, we tested the levels of phosphorylated (active form) p44/p42 MAPK (here referred to as ERK1/2; also known as Mapk3/Mapk1). Importantly, we found that WT pancreatic cells located at the branch tips displayed significantly higher levels of pERK1/2 than did cells in the trunk both *in vivo* and *ex vivo* in organ cultures (Fig. 5A,B). To address whether this differential distribution of pERK1/2 is required for the growth of epithelial branches, we pharmacologically inhibited the kinase activities of ERKs by using the selective compound PD0325901 (Bain et al., 2007) in WT pancreatic explants (Fig. 5C). Strikingly, samples cultured for two days in the presence of PD0325901 were smaller than untreated WT pancreatic epithelium, and displayed a smooth surface with no signs of branching (Fig. 5B,C).

Accordingly, we detected a reduction in cell proliferation in PD0325901-treated WT pancreatic cultures, exhibiting 50% and 60% decrease in the average number of pHH3$^{+}$ cells after 24-hour and 48-hour exposure, respectively (Fig. 5F). However, these defects were not accompanied by obvious and measurable changes in F-actin cytoskeleton organisation (data not shown), suggesting that ERK controls primarily proliferation.

Because epithelial tip structures did not form in the absence of *Stard13*, we investigated next the possibility that *Stard13*$^{PA\text{-}deleted}$ pancreatic cells display reduced pERK activity or loss of its spatial distribution. Both immunostaining and western blot analyses showed that the levels of pERK1/2 proteins were substantially reduced in embryonic pancreas upon *Stard13* ablation, whereas total ERK, PI3K-Akt and FAK (Ptk2) pathways were unaffected (Fig. 5D,G,H). Importantly, specific inhibition of Rho by C3 rescued branch-tip formation in *Stard13*$^{PA\text{-}deleted}$ pancreatic explants, restoring pERK activation and cell proliferation to levels similar to WT (Fig. 3; Fig. 5E-G). These results suggest that proliferation of progenitors at the newly formed tips is supported by local activation of the ERK signalling.

The integrin-FAK signalling axis is known for regulating proliferation through the control of ERK (MAPK) pathway (Legate et al., 2009). However, the levels of FAK-Y397 phosphorylation, integrin signalling and, in general, cell-ECM adhesion were unchanged in the absence of *Stard13* in the pancreatic epithelium (Fig. 5H-J). Thus, this mechanism does not appear to contribute to ERK regulation in pancreatic progenitor proliferation in the absence of *Stard13*.

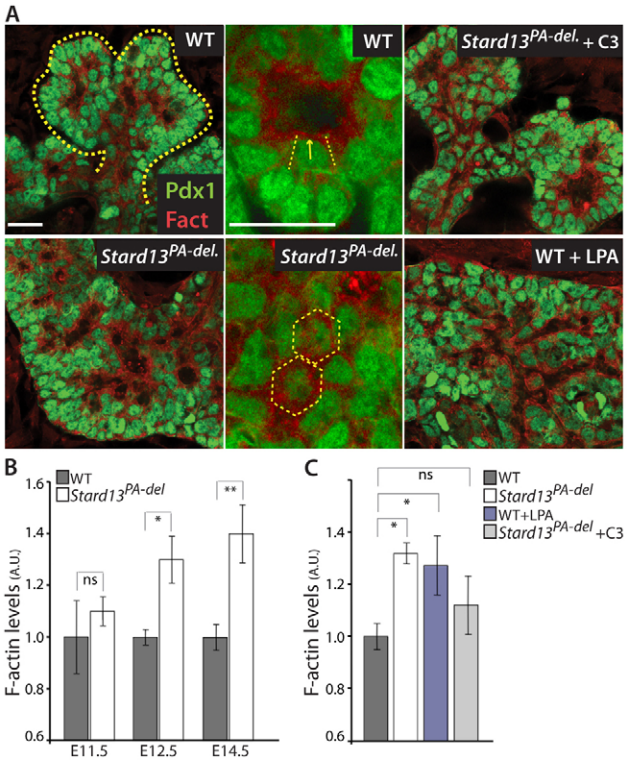


**Fig. 4. Aberrant F-actin network distribution in *Stard13*$^{PA\text{-}deleted}$ pancreatic epithelium.** (**A**) Whole-mount immunostaining for Pdx1 and F-actin on WT, untreated *Stard13*$^{PA\text{-}deleted}$ and C3-treated *Stard13*$^{PA\text{-}deleted}$, and LPA-treated WT explants. Arrows in indicate F-act apical distribution in WT cells. Note that F-act apical distribution is lost in LPA-treated WT and *Stard13*$^{PA\text{-}deleted}$ explants, whereas it is restored in explants rescued with C3 treatment. Yellow dotted outline delineates pancreatic tip in WT. Dotted hexagonal outlines indicate the cell contour in the mutant pancreas. Biological activity of LPA was tested on embryonic fibroblasts and WT pancreatic explants (supplementary material Fig. S5). Scale bars: 20 μm. (**B**) Quantification of actin filament staining from confocal images of pancreatic epithelia at E11.5, E12.5 and E14.5. Average fluorescence intensity was measured in Pdx1$^{+}$ area of interest after background subtraction using ImageJ. The given intensity values for each developmental stage were normalised to the corresponding WT levels (set to 1). (**C**) Histogram showing relative intensity of F-actin in WT, LPA-treated WT, untreated *Stard13*$^{PA\text{-}deleted}$ and C3-treated *Stard13*$^{PA\text{-}deleted}$ explants. A.U., arbitrary units. Error bars indicate s.e.m.; $n \geq 3$ experiments. *$P<0.05$, **$P<0.01$, determined by Student's *t*-test. ns, not significant.

Next, we sought to establish whether cell-shape changes and actin cytoskeleton might directly influence proliferation in the pancreatic epithelium. Actin polymerisation and F-actin filaments accumulation can control gene expression through regulation of MAL/SRF transcriptional activity (Descot et al., 2009; Posern and Treisman, 2006). Strikingly, we found induction of several MAL/SRF downstream effectors, including *Srf*, *Ctgf* and *Vcl*, in the *Stard13*$^{PA\text{-}deleted}$ embryonic pancreas (Fig. 6A). By contrast, mesenchymal MAL/SRF targets, such as *Acta2*, or TCF-dependent SRF targets, such as *Fos*, were not detectable (Descot et al., 2009) (data not shown). Among the induced MAL/SRF targets, we found some with known anti-proliferative function, such as *Mig6* (also know as *Erffi1*) and *Zfp36* (Descot et al., 2009). Intriguingly, both *Mig6* and *Zfp36* are known negative regulators of EGF/MAPK signalling, acting at different levels of the cascade (Descot et al., 2009; Ferby et al., 2006), and they were expressed at very low, almost undetectable, levels in WT embryonic pancreas, but readily accumulated in mutant cells (Fig. 6A,B). To address directly whether SRF transcriptional activation downstream of Rho and actin polymerisation is responsible of the proliferation defects in the *Stard13*$^{PA\text{-}deleted}$ pancreatic epithelium, we inhibited Rho transcriptional signalling using the Rho/SRF pathway inhibitor CCG-1423 (Evelyn et al., 2007). Treatment of *Stard13*$^{PA\text{-}deleted}$ pancreatic explants with the compound CCG-1423 partially restored the formation of primary branches that expanded in overall size compared with untreated *Stard13*$^{PA\text{-}deleted}$ explants (Fig. 6C,D). These results imply that selective disruption of Rho/SRF transcriptional activity is able to rescue proliferation defects in the absence of the RhoGAP Stard13, even though its effect is more modest than that of upstream functional inhibition of Rho signalling, for instance through C3-ribosyltransferase treatment (Figs 3-5).

As *Ctgf* is a common target for activated MAL/SRF and Hippo/Yap signalling pathways and as Yap is modulated by high tissue stiffness and by Rho activity (Dupont et al., 2011; Wada et al., 2011), we also examined the activity status and subcellular localisation of the two mammalian components of the Hippo organ-growth pathway, Yap and phosphorylated Yap (p-Yap), in the embryonic pancreas. Both Yap and p-Yap levels and distribution were unchanged in the *Stard13*$^{PA\text{-}deleted}$ tissue compared with WT (Fig. 6E). These observations indicate that, despite active Rho and F-actin fibre accumulation in the absence of *Stard13*, there is no Yap modulation in the mutant pancreatic epithelium, in contrast to what has been reported in mesenchymal cells (Dupont et al., 2011; Wada et al., 2011). By contrast, our data suggest that F-actin accumulation converges into the MAPK cascade through SRF targets, providing a mechanistic explanation for the reduced pERK levels in *Stard13*$^{PA\text{-}deleted}$ pancreatic epithelium (Fig. 6).

## DISCUSSION

Collectively, our findings indicate that the RhoGAP Stard13 temporally and spatially regulates Rho activity in the developing pancreas to ensure that morphogenesis and establishment of tissue architecture are coordinated with organ growth (Fig. 6F).

Precise spatiotemporal regulation of Rho activity is a prerequisite for proper assembly and tension of the actomyosin cytoskeleton (Van Aelst and Symons, 2002; Etienne-Manneville and Hall, 2002). Accordingly, uninhibited Rho activity in Stard13$^{PA\text{-}deleted}$ embryos has a profound impact on the organisation of the actomyosin network, which in turn hampers epithelial remodelling events, including cell-shape changes, cell arrangement in rosette-like structures and microlumen connection, in the developing pancreas. These results unveil a novel role for actin cytoskeletal dynamics at the onset of pancreatic branching morphogenesis. Hence, it is likely that Rho-dependent actomyosin contraction plays distinct roles regulating (1) concerted apical constriction and (2) subsequent resolution of the 'rosette-like' structures into elongating tubules. The formation of multicellular rosettes provides an efficient mechanism for rearrangement of cells into a single epithelial layer (Zallen and Blankenship, 2008). Similarly to other elongating epithelia, we have found multicellular 'rosette-like' structures in the pancreatic epithelium at the time at which epithelial remodelling starts, suggesting that rosette arrangements might contribute to the transition from stratified to monolayered epithelium in the pancreas too.

Our findings suggest that Rho activity in the developing pancreas is unique and not redundant with Cdc42 GTPase, which is instead required for initiating microlumen formation and apical-basolateral cell polarity (Kesavan et al., 2009). Establishment of cell polarity is

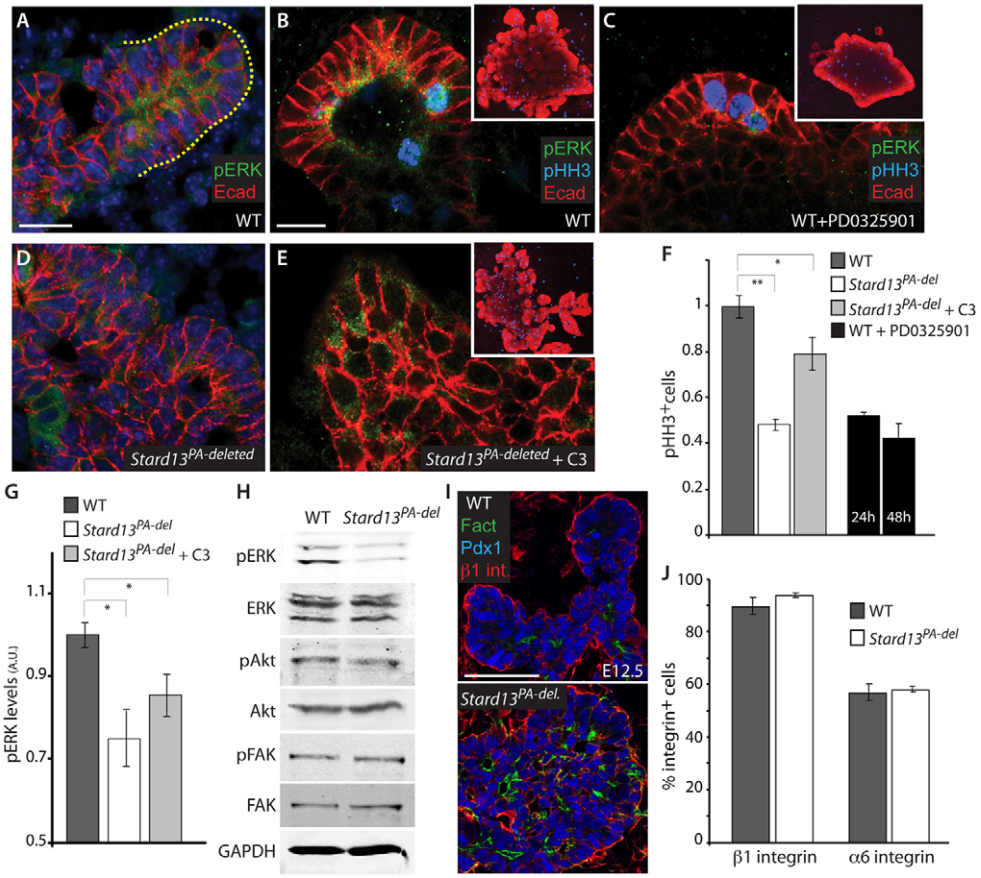


**Fig. 5. Active pERK signalling accumulates at the tip of the branches in the developing pancreas.** (**A-E**) Immunodetection of pERK1/2 and Ecad on cryosections of E12.5 WT (A) and *Stard13*$^{PA\text{-}deleted}$ (D) pancreas and whole-mount WT (B), PD032590-treated WT (C) and C3-treated *Stard13*$^{PA\text{-}deleted}$ (E) pancreatic explants. Insets are lower magnification micrographs of B, C and E maximum confocal *z*-projections. Yellow dotted outline delineates pancreatic tip. (**F**) Quantification of pHH3$^{+}$ cells in WT, *Stard13*$^{PA\text{-}deleted}$, PD0325901-treated WT and C3-treated *Stard13*$^{PA\text{-}deleted}$ pancreatic explants. Relative number of pHH3$^{+}$ cells versus total volume of the pancreatic explant (Ecad$^{+}$) was calculated. *n*=3. (**G**) Histogram showing relative intensity of pERK in WT, untreated *Stard13*$^{PA\text{-}deleted}$ and C3-treated *Stard13*$^{PA\text{-}deleted}$ explants. A.U., arbitrary units. (**H**) Western blot analysis of WT and *Stard13*$^{PA\text{-}deleted}$ pancreatic lysates probed with the indicated antibodies. (**I**) Immunostaining of β1-integrin (β1 int.) in E12.5 WT and *Stard13*$^{PA\text{-}deleted}$ pancreas. (**J**) FACS quantification of integrin protein levels in E13.5 pancreatic cells. The histogram depicts the percentage of pancreatic cell populations with β1-integrin and α6-integrin protein expression. *n*=3. Error bars represent ± s.e.m. **P*<0.05, ***P*<0.01, determined by Student's *t*-test. Scale bars: in A,B, 20 µm; in I, 50 µm.

regulated by proper sorting and delivery of proteins to different membranes and by conserved signalling complexes, such as the Par, Crumbs and Scribble complexes (Nelson, 2009). Cdc42 is known to establish a functional and mature apical surface by interacting with the Par3-Par6-aPKC polarity complex protein (Van Aelst and Symons, 2002; Etienne-Manneville and Hall, 2002; Kesavan et al., 2009). Upon *Cdc42* ablation, pancreatic epithelium fails to generate multicellular common apical surfaces, forming instead autocellular lumens, ultimately resulting in a fragmented epithelium without tubes (Kesavan et al., 2009). By contrast, misregulation of Rho signalling in *Stard13*$^{PA\text{-}deleted}$ pancreas does not result in autocellular lumen formation, and apical-basolateral (e.g. PKCζ/mucin/laminin) polarity is established in *Stard13* mutant epithelium, despite the morphogenetic defects. Taken together, these findings suggest an opposite activity of Rho and Cdc42 GTPases in the developing pancreas that might account for the different pancreatic phenotypes of *Cdc42* and *Stard13* mutants: fragmented epithelium in the former and globular stratified epithelium in the latter. However, this does not exclude potential crosstalk among different GTPases during pancreatic morphogenesis, as previously described in other contexts (Yamada and Nelson, 2007; Yu et al., 2008).

The mechanisms that regulate pancreatic organ size remain poorly understood. Recent observations have shown that the number of pancreatic progenitors is established early in development by an intrinsic programme and this would dictate final organ size (Stanger et al., 2007; Zhou et al., 2007). At the onset of pancreatic morphogenesis, distal tips of the branching epithelium contain fast-proliferating progenitors and, possibly, define a special supporting 'niche', as shown in other epithelial organs (Hogan and Kolodziej, 2002; Horb and Slack, 2000; Watanabe and Costantini, 2004; Zhou et al., 2007). Interestingly, ablation of *Stard13*, expression of which is enriched at the distal tips, results in pancreatic hypoplasia. Based on our findings, we propose Stard13 as an intrinsic regulator of the number of pancreatic progenitors through the establishment of the pancreatic tip domain. From a mechanistic point of view, our data define a reciprocal interaction between actin-MAL/SRF signalling and MAPK signalling to locally regulate progenitor-cell proliferation in the pancreas (Fig. 6F). As such, the initial progenitor pool can expand and reach its proper final size, which predetermines pancreas organ size in the adult (Stanger et al., 2007; Zhou et al., 2007). By contrast, in the absence of *Stard13*, constitutively active Rho/actin signalling not only has disruptive effects on tip

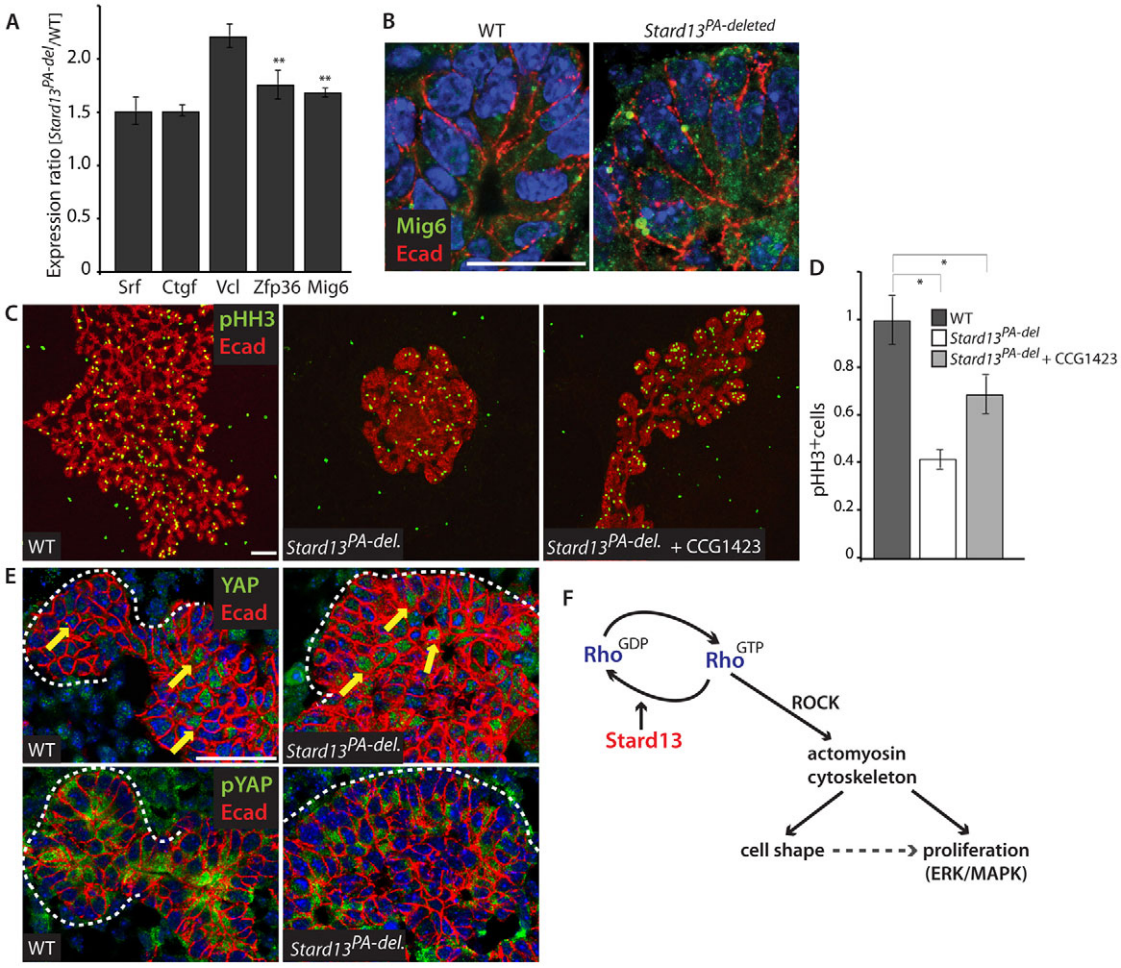


**Fig. 6. Activation of actin-MAL/SRF signalling in *Stard13*$^{PA\text{-}deleted}$ pancreatic epithelium.** (**A**) Quantitative real-time RT-PCR analysis of indicated MAL/SRF target genes in E14.5 WT and *Stard13*$^{PA\text{-}deleted}$ pancreas. Data were normalised to that of 36B4 and SDHA and shown as expression ratio (2-log values) of *Stard13*$^{PA\text{-}deleted}$ versus WT pancreas. Error bars represent ± s.e.m. (**B**) Immunodetection of Mig6 on cryosections of E12.5 WT and *Stard13*$^{PA\text{-}deleted}$ pancreas. Blue, Hoechst nuclear counterstain. (**C**) Representative maximum confocal *z*-projections of Ecad and pHH3 immunofluorescence analysis in WT, *Stard13*$^{PA\text{-}deleted}$ and CCG1423-treated *Stard13*$^{PA\text{-}deleted}$ pancreatic explants. (**D**) Quantification of pHH3$^{+}$ cells in WT, *Stard13*$^{PA\text{-}deleted}$ and CCG1423-treated *Stard13*$^{PA\text{-}deleted}$ pancreatic explants. Relative number of pHH3$^{+}$ cells versus total volume of the pancreatic explant (Ecad$^{+}$) was calculated. $n$=3. Error bars represent ± s.e.m. (**E**) Immunostaining analysis of Yap, p-Yap and Ecad on WT and *Stard13*$^{PA\text{-}deleted}$ E12.5 pancreas. Yellow arrows indicate cells displaying nuclear Yap localisation throughout the WT and *Stard13*$^{PA\text{-}deleted}$ pancreatic epithelia. Blue, Hoechst nuclear counterstain. White dotted outlines delineate pancreatic epithelium. (**F**) Working model consistent with the data presented. Our finding suggests that the RhoGAP Stard13 is required to temporally and spatially regulate Rho activity in the developing pancreas to ensure that morphogenesis and establishment of tissue architecture are coordinated with organ growth. *$P$<0.05, **$P$<0.01, determined by Student's $t$-test. Scale bars: in B, 20 µm; in C, 100 µm; in E, 50 µm.

morphogenesis but also locally reduces active pERK, through MAL/SRF transcriptional regulation, eventually resulting in organ hypoplasia. The temporal succession of events proposed in our model is in line with the fact that aberrant cell shape and F-actin accumulation are the earliest detectable defects in the mutant pancreas, whereas reduction in cell proliferation becomes obvious at E12.5. Importantly, we also show that selective inhibition of downstream Rho/SRF transcriptional signalling rescues the *Stard13* mutant cell proliferation defects, to some extent. Nevertheless, upstream inhibition of the Rho signalling using the C3 exotoxin molecule results in a more effective rescue of the *Stard13*$^{PA\text{-}deleted}$ defects than does transcriptional disruption of the pathway using CCG1423. These observations reinforce the notion that cell shape and cytoskeleton are at the origin of the phenotypic defects in the *Stard13* mutant, being not completely eliminated by a downstream rescue at the transcriptional level. Also, these results suggest possible mechanical effects of cell shape and actomyosin cytoskeleton on cell division in the developing pancreas that might be independent of the SRF/MAPK pathway.

Overall, this study presents an unprecedented mechanism for integrating morphogenesis and growth by combining localised control of actin cytoskeleton and growth factor signalling. Full understanding of the relationship between pancreatic progenitor cells and tissue architecture will help in defining the signals that are necessary for maintenance of the progenitor pool or differentiation into a particular lineage. Better understanding of these concepts will have practical implications for any possible cell-based therapy of diabetes based on expansion of pancreatic progenitors and generation of insulin producing β-cells from stem cells or progenitor cells.

**Acknowledgements**
We thank Ali H. Brivanlou for invaluable input into the study and contribution to the initiation of the work. We thank all members of the Spagnoli laboratory for discussion. We are grateful to C. Birchmeier, W. Birchmeier, M. Schober and M. E. Torres-Padilla for helpful comments on the manuscript; D. A. Melton for the *Pdx1-Cre* transgenic strain; to M. Sander for anti-Ngn3 antibody; M. Wegner for anti-Sox9 antibody; and A. Sprinkel for anti-Ptf1a antibody.

**Funding**
This research was supported by institutional funds from the Helmholtz Association and the FP7-IRG-2008-ENDOPANC grant. F.M.S. is recipient of ERC-2009-Starting HEPATOPANCREATIC Grant.

**Competing interests statement**
The authors declare no competing financial interests.

**Supplementary material**
Supplementary material available online at
http://dev.biologists.org/lookup/suppl/doi:10.1242/dev.082701/-/DC1

**References**

**Bain, J., Plater, L., Elliott, M., Shpiro, N., Hastie, C. J., McLauchlan, H., Klevernic, I., Arthur, J. S., Alessi, D. R. and Cohen, P.** (2007). The selectivity of protein kinase inhibitors: a further update. *Biochem. J.* **408**, 297-315.
**Bhushan, A., Itoh, N., Kato, S., Thiery, J. P., Czernichow, P., Bellusci, S. and Scharfmann, R.** (2001). Fgf10 is essential for maintaining the proliferative capacity of epithelial progenitor cells during early pancreatic organogenesis. *Development* **128**, 5109-5117.
**Bishop, A. L. and Hall, A.** (2000). Rho GTPases and their effector proteins. *Biochem. J.* **348**, 241-255.
**Cascone, I., Audero, E., Giraudo, E., Napione, L., Maniero, F., Philips, M. R., Collard, J. G., Serini, G. and Bussolino, F.** (2003). Tie-2-dependent activation of RhoA and Rac1 participates in endothelial cell motility triggered by angiopoietin-1. *Blood* **102**, 2482-2490.
**Descot, A., Hoffmann, R., Shaposhnikov, D., Reschke, M., Ullrich, A. and Posern, G.** (2009). Negative regulation of the EGFR-MAPK cascade by actin-MAL-mediated Mig6/Errfi-1 induction. *Mol. Cell* **35**, 291-304.
**Dupont, S., Morsut, L., Aragona, M., Enzo, E., Giulitti, S., Cordenonsi, M., Zanconato, F., Le Digabel, J., Forcato, M., Bicciato, S. et al.** (2011). Role of YAP/TAZ in mechanotransduction. *Nature* **474**, 179-183.
**Edlund, H.** (2002). Pancreatic organogenesis – developmental mechanisms and implications for therapy. *Nat. Rev. Genet.* **3**, 524-532.
**Etienne-Manneville, S. and Hall, A.** (2002). Rho GTPases in cell biology. *Nature* **420**, 629-635.
**Evelyn, C. R., Wade, S. M., Wang, Q., Wu, M., Iñiguez-Lluhí, J. A., Merajver, S. D. and Neubig, R. R.** (2007). CCG-1423: a small-molecule inhibitor of RhoA transcriptional signaling. *Mol. Cancer Ther.* **6**, 2249-2260.
**Ferby, I., Reschke, M., Kudlacek, O., Knyazev, P., Pantè, G., Amann, K., Sommergruber, W., Kraut, N., Ullrich, A., Fässler, R. et al.** (2006). Mig6 is a negative regulator of EGF receptor-mediated skin morphogenesis and tumor formation. *Nat. Med.* **12**, 568-573.
**Gu, G., Dubauskaite, J. and Melton, D. A.** (2002). Direct evidence for the pancreatic lineage: NGN3+ cells are islet progenitors and are distinct from duct progenitors. *Development* **129**, 2447-2457.
**Hammar, E., Tomas, A., Bosco, D. and Halban, P.** (2009). Role of the Rho-ROCK (Rho-Associated Kinase) signaling pathway in the regulation of pancreatic beta-cell function. *Endocrinology* **150**, 2072-2079.
**Hick, A. C., Eyll, J. M., Cordi, S., Forez, C., Passante, L., Kohara, H., Nagasawa, T., Vanderhaeghen, P., Courtoy, P. J., Rousseau, G. G. et al.** (2009). Mechanism of primitive duct formation in the pancreas and submandibular glands: a role for SDF-1. *BMC Dev. Biol.* **9**, 66.
**Hogan, B. L. M. and Kolodziej, P. A.** (2002). Organogenesis: molecular mechanisms of tubulogenesis. *Nat. Rev. Genet.* **3**, 513-523.
**Horb, L. D. and Slack, J. M.** (2000). Role of cell division in branching morphogenesis and differentiation of the embryonic pancreas. *Int. J. Dev. Biol.* **44**, 791-796.
**Jensen, J.** (2004). Gene regulatory factors in pancreatic development. *Dev. Dyn.* **229**, 176-200.
**Kawaguchi, Y., Cooper, B., Gannon, M., Ray, M., MacDonald, R. J. and Wright, C. V.** (2002). The role of the transcriptional regulator Ptf1a in converting intestinal to pancreatic progenitors. *Nat. Genet.* **32**, 128-134.
**Kesavan, G., Sand, F. W., Greiner, T. U., Johansson, J. K., Kobberup, S., Wu, X., Brakebusch, C. and Semb, H.** (2009). Cdc42-mediated tubulogenesis controls cell specification. *Cell* **139**, 791-801.
**Kuure, S., Cebrian, C., Machingo, Q., Lu, B. C., Chi, X., Hyink, D., D'Agati, V., Gurniak, C., Witke, W. and Costantini, F.** (2010). Actin depolymerizing factors cofilin1 and destrin are required for ureteric bud branching morphogenesis. *PLoS Genet.* **6**, e1001176.
**Legate, K. R., Wickström, S. A. and Fässler, R.** (2009). Genetic and cell biological analysis of integrin outside-in signaling. *Gend. Dev.* **23**, 397-418.
**Leung, T. H.-Y., Ching, Y.-P., Yam, J. W. P., Wong, C.-M., Yau, T.-O., Jin, D.-Y. and Ng, I. O.-L.** (2005). Deleted in liver cancer 2 (DLC2) suppresses cell transformation by means of inhibition of RhoA activity. *Proc. Natl. Acad. Sci. USA* **102**, 15207-15212.
**Lu, P. and Werb, Z.** (2008). Patterning mechanisms of branched organs. *Science* **322**, 1506-1509.
**Malliri, A., Klooster, J. P., Olivo, C. and Collard, J. G.** (2002). Determination of the activity of Rho-like GTPases in cells. In *Methods in Molecular Biology*, *GTPase Protocols: The Ras Superfamily*, Vol. 189 (ed. T. E. J. Manser and T. Leung), pp. 99-109. Totowa, NJ: Humana Press.
**Metzger, R. J., Klein, O. D., Martin, G. R. and Krasnow, M. A.** (2008). The branching programme of mouse lung development. *Nature* **453**, 745-750.
**Nelson, W. J.** (2009). Remodeling epithelial cell organization: transitions between front-rear and apical-basal polarity. *Cold Spring Harb. Perspect. Biol.* **1**, a000513.
**Pan, F. C. and Wright, C.** (2011). Pancreas organogenesis: from bud to plexus to gland. *Dev. Dyn.* **240**, 530-565.
**Petzold, K. M. and Spagnoli, F. M.** (2012). A system for *ex vivo* culturing of embryonic pancreas. *J. Vis. Exp.* **66**, 3979.
**Pfaffl, M. W., Horgan, G. W. and Dempfle, L.** (2002). Relative expression software tool (REST©) for group-wise comparison and statistical analysis of relative expression results in real-time PCR. *Nucleic Acids Res.* **30**.
**Posern, G. and Treisman, R.** (2006). Actin' together: serum response factor, its cofactors and the link to signal transduction. *Trends Cell Biol.* **16**, 588-596.
**Puri, S. and Hebrok, M.** (2007). Dynamics of embryonic pancreas development using real-time imaging. *Dev. Biol.* **306**, 82-93.
**Puri, S. and Hebrok, M.** (2010). Cellular plasticity within the pancreas—lessons learned from development. *Dev. Cell* **18**, 342-356.
**Rodriguez, C. I., Buchholz, F., Galloway, J., Sequerra, R., Kasper, J., Ayala, R., Stewart, F. A. and Dymecki, S. M.** (2000). High-efficiency deleter mice show that FLPe is an alternative to Cre-loxP. *Nat. Genet.* **25**, 139-140.
**Schaeren-Wiemers, N. and Gerfin-Moser, A.** (1993). A single protocol to detect transcripts of various types and expression levels in neural tissue and cultured cells: *in situ* hybridization using digoxigenin-labelled cRNA probes. *Histochemistry* **100**, 431-440.
**Schwenk, F., Baron, U. and Rajewsky, K.** (1995). A cre-transgenic mouse strain for the ubiquitous deletion of loxP-flanked gene segments including deletion in germ cells. *Nucleic Acids Res.* **23**, 5080-5081.
**Seymour, P. A., Freude, K. K., Tran, M. N., Mayes, E. E., Jensen, J., Kist, R., Scherer, G. and Sander, M.** (2007). SOX9 is required for maintenance of the pancreatic progenitor cell pool. *Proc. Natl. Acad. Sci. USA* **104**, 1865-1870.
**Sordella, R., Jiang, W., Chen, G.-C., Curto, M. and Settleman, J.** (2003). Modulation of Rho GTPase signaling regulates a switch between adipogenesis and myogenesis. *Cell* **113**, 147-158.
**Soriano, P.** (1999). Generalized lacZ expression with the ROSA26 Cre reporter strain. *Nat. Genet.* **21**, 70-71.
**Spagnoli, F. M.** (2007). From endoderm to pancreas: a multistep journey. *Cell. Mol. Life Sci.* **64**, 2378-2390.
**Spagnoli, F. M. and Brivanlou, A. H.** (2006). The RNA-binding protein, Vg1RBP, is required for pancreatic fate specification. *Dev. Biol.* **292**, 442-456.
**Stanger, B. Z., Tanaka, A. J. and Melton, D. A.** (2007). Organ size is limited by the number of embryonic progenitor cells in the pancreas but not the liver. *Nature* **445**, 886-891.
**Tcherkezian, J. and Lamarche-Vane, N.** (2007). Current knowledge of the large RhoGAP family of proteins. *Biol. Cell* **99**, 67-86.
**Valenzuela, D. M., Murphy, A. J., Frendewey, D., Gale, N. W., Economides, A. N., Auerbach, W., Poueymirou, W. T., Adams, N. C., Rojas, J., Yasenchak, J. et al.** (2003). High-throughput engineering of the mouse genome coupled with high-resolution expression analysis. *Nat. Biotechnol.* **21**, 652-659.
**Van Aelst, L. and Symons, M.** (2002). Role of Rho family GTPases in epithelial morphogenesis. *Genes Dev.* **16**, 1032-1054.
**Villasenor, A., Chong, D. C., Henkemeyer, M. and Cleaver, O.** (2010). Epithelial dynamics of pancreatic branching morphogenesis. *Development* **137**, 4295-4305.
**Wada, K., Itoga, K., Okano, T., Yonemura, S. and Sasaki, H.** (2011). Hippo pathway regulation by cell morphology and stress fibers. *Development* **138**, 3907-3914.
**Watanabe, T. and Costantini, F.** (2004). Real-time analysis of ureteric bud branching morphogenesis *in vitro*. *Dev. Biol.* **271**, 98-108.
**Yamada, S. and Nelson, W. J.** (2007). Localized zones of Rho and Rac activities drive initiation and expansion of epithelial cell-cell adhesion. *J. Cell Biol.* **178**, 517-527.
**Yu, W., Shewan, A. M., Brakeman, P., Eastburn, D. J., Datta, A., Bryant, D. M., Fan, Q.-W., Weiss, W. A., Zegers, M. M. and Mostov, K. E.** (2008). Involvement of RhoA, ROCK I and myosin II in inverted orientation of epithelial polarity. *EMBO Rep.* **9**, 923-929.
**Zallen, J. A. and Blankenship, J. T.** (2008). Multicellular dynamics during epithelial elongation. *Semin. Cell Dev. Biol.* **19**, 263-270.
**Zhou, Q., Law, A. C., Rajagopal, J., Anderson, W. J., Gray, P. A. and Melton, D. A.** (2007). A multipotent progenitor domain guides pancreatic organogenesis. *Dev. Cell* **13**, 103-114.

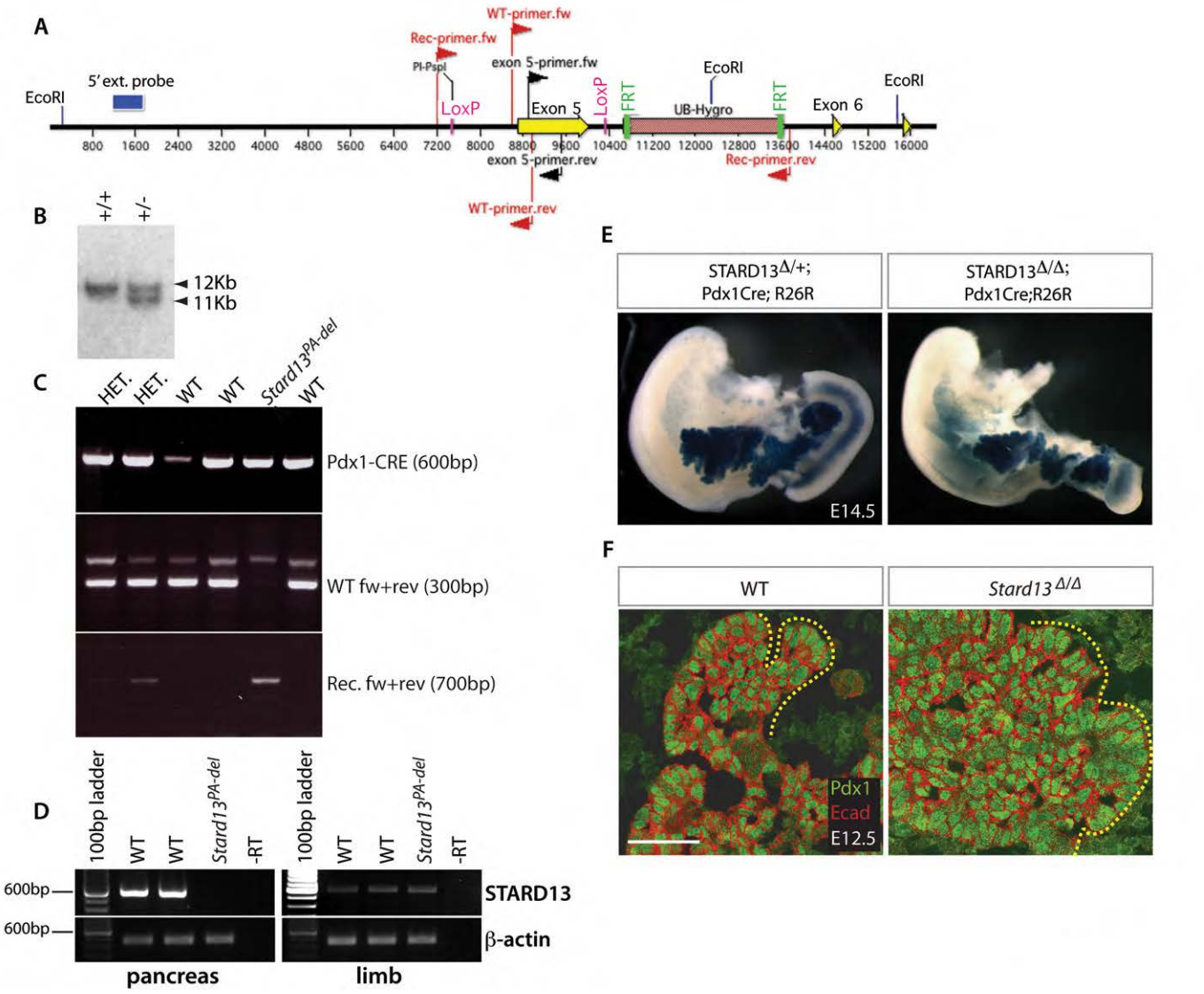


**Fig. S1. Generation of pancreas-specific *Stard13*$^{PA\text{-}deleted}$ mice.** (**A**) Schematic representation of the targeted *Stard13*$^{flox}$ allele, indicating the loxP sites (in pink) flanking exon 5 of the gene, FRT-flanked-Hygromicin, *Eco*RI restriction sites, 5′ external probe (blue) and primers used for genotyping. Upon Cre-mediated recombination, excision of exon 5, which codes for amino acid residues 12-453, would fully inactivate the gene, introducing a frameshift mutation and premature stop codon, which results in a null *Stard13* allele. (**B**) Targeted ES cells and founder mice tails were identified by Southern blot analysis with restriction enzyme *Eco*RI and 5′ external probe. Upon digestion of genomic DNA with *Eco*RI, expected shift in size between WT (12.3 kb) and targeted (11.7 kb) allele was detected. (**C**) Deletion *in vivo* of the conditional allele in *Stard13*$^{flox/flox}$; *Pdx1-Cre* pancreatic cells. PCR on genomic DNA of E18.5 pancreatic rudiments for *Pdx1-Cre* transgene, wild-type (WT fw+rev primers) and recombined allele (Rec. fw+rev primers). In *Stard13*$^{PA\text{-}deleted}$ that carries the *Pdx1-Cre* transgene the recombined allele, but not the wild-type allele, was amplified, whereas the wild-type allele was detected in controls (HET or WT). (**D**) RT-PCR analysis of *Stard13* in pancreatic and forelimb tissue from WT and *Stard13*$^{PA\text{-}deleted}$ E14.5 embryos detected the transcript in both WT tissues, in the forelimb of *Stard13*$^{PA\text{-}deleted}$ embryos, but not in *Stard13*$^{PA\text{-}deleted}$ pancreas, indicating tissue-specific gene ablation. β-actin was used as control. (**E**) X-Gal staining in both *Stard13*$^{\Delta/+}$; *Pdx1-Cre*; ROSA26R$^{+/-}$ and *Stard13*$^{\Delta/\Delta}$; *Pdx1-Cre*; ROSA26R$^{+/-}$ indicated efficient Cre recombination, showing almost uniform blue staining in the pancreas at E14.5. R26R indicator mice were obtained from the Jackson Laboratory [Gt(ROSA)26Sortm1Sor] (Soriano, 1999). Pancreatic size difference was evident between HET and mutant. (**F**) Immunofluorescence analysis of E12.5 WT and *Stard13*$^{\Delta/\Delta}$ pancreases using antibodies against Pdx1 and E-cadherin (Ecad). Deletion of *Stard13* in all tissues (*Stard13*$^{\Delta}$) using the CMV-Cre transgenic strain (Schwenk et al., 1995) led to a pancreatic-specific phenotype as observed in *Stard13*$^{PA\text{-}deleted}$ embryos, suggesting a tissue-specific activity of the RhoGAP Stard13. Scale bar: 50 μm.

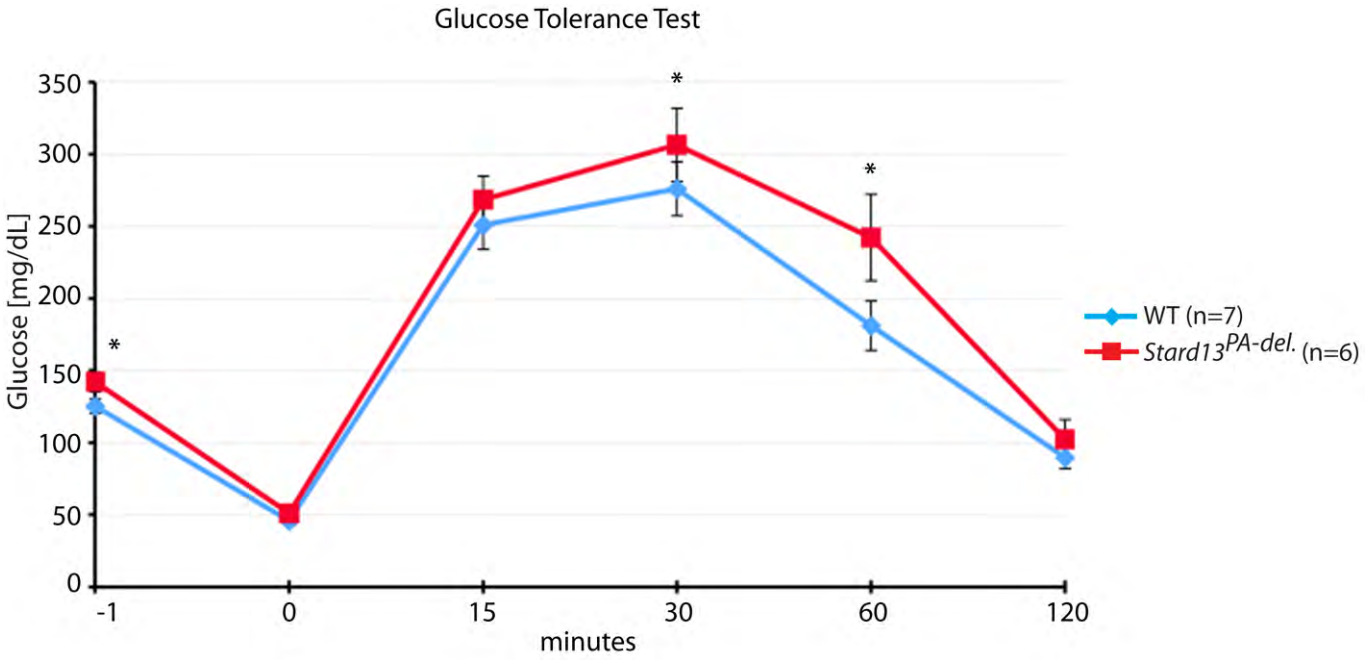


**Fig. S2. Loss of *Stard13* leads to a mild glucose intolerance adult phenotype.** Glucose levels were measured from blood collected from the tail immediately before the glucose challenge (time point 0) and 15, 30, 60 and 120 minutes after the glucose injection using a blood glucose meter (Contour, Bayer). Data are expressed as means ± s.e.m. The level of statistical significance was determined using Student's two-tailed *t*-test when the difference between the means of two populations was considered. $P<0.05$ was considered statistically significant. These results are in line with previous observations (Hammar et al., 2009). Finally, defects in glucose metabolism might explain the postnatal growth retardation that we observed in *Stard13*$^{PA\text{-}deleted}$ animals.

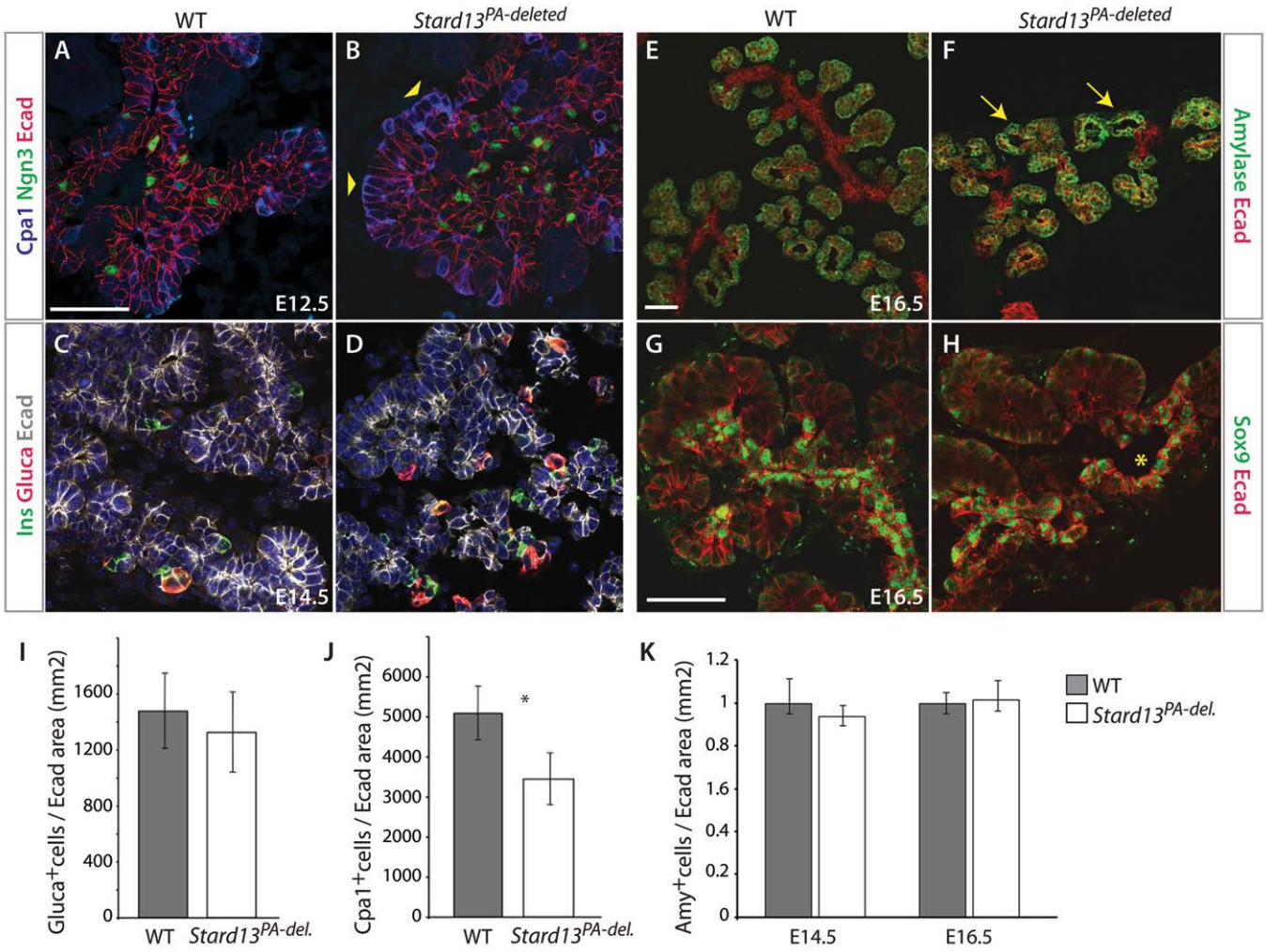


**Fig. S3. *Stard13* ablation does not influence pancreatic lineage allocation.** WT and *Stard13*$^{PA\text{-}deleted}$ pancreas sections were stained with antibodies against the three main pancreatic cell lineages. (**A**) The transcription factor *Ngn3* (*Neurog3*) is the earliest recognisable marker of endocrine progenitors, which subsequently give rise to mature endocrine cells. In the E12.5 WT, Ngn3+ (green) and Cpa1+ cells (blue) displayed typical distribution in the trunk and at the tips of the branching epithelium, respectively. (**B**) In the *Stard13*$^{PA\text{-}deleted}$ Ngn3+ cells trunk location was maintained, whereas Cpa1+ cells distribution was disorganised (arrowheads). (**C**,**D**) Endocrine cells expressing insulin (Ins) or glucagon (Gluca) cells were detected in both WT (C) and *Stard13*$^{PA\text{-}deleted}$ (D) E14.5 pancreases. Blue, Hoechst nuclear counterstain. (**E-H**) At E16.5, exocrine cells (amylase+) and duct cells (Sox9+) were found in both WT (E,G) and *Stard13*$^{PA\text{-}deleted}$ pancreases (F,H). Arrows indicate malformed acini (F) in the *Stard13*$^{PA\text{-}deleted}$ pancreas. The ductal network architecture was severely perturbed, showing discontinuous ducts (asterisk) and absence of typical branching tree-pattern in the mutant (H). (**I**) Quantification of differentiated endocrine cells (Gluca+) versus total Ecad+ area showed no change. *n*=3. (**J**) Quantification of progenitor Cpa1+ cells versus total Ecad+ area showed reduction in *Stard13*$^{PA\text{-}deleted}$ at E14.5, which is consistent with their decreased proliferative activity at E12.5 (Fig. 1F). Similarly, 30% reduction of Cpa1+ cells versus Pdx1+ cells was measured in the mutant pancreas (Cpa1+/Pdx1+cells in E14.5 *Stard13*$^{PA\text{-}deleted}$ pancreas=20±3.2 %; Cpa1+/Pdx1+cells in E14.5 WT pancreas=30±4 %). n=3. (**K**) No difference was observed in the relative number of exocrine cells (Amy+/Ecad+) between WT and *Stard13*$^{PA\text{-}deleted}$ pancreas at E14.5 and E16.5. *n*=3. Error bars represent ± s.e.m. **P*<0.05. Scale bars: 50 μm.

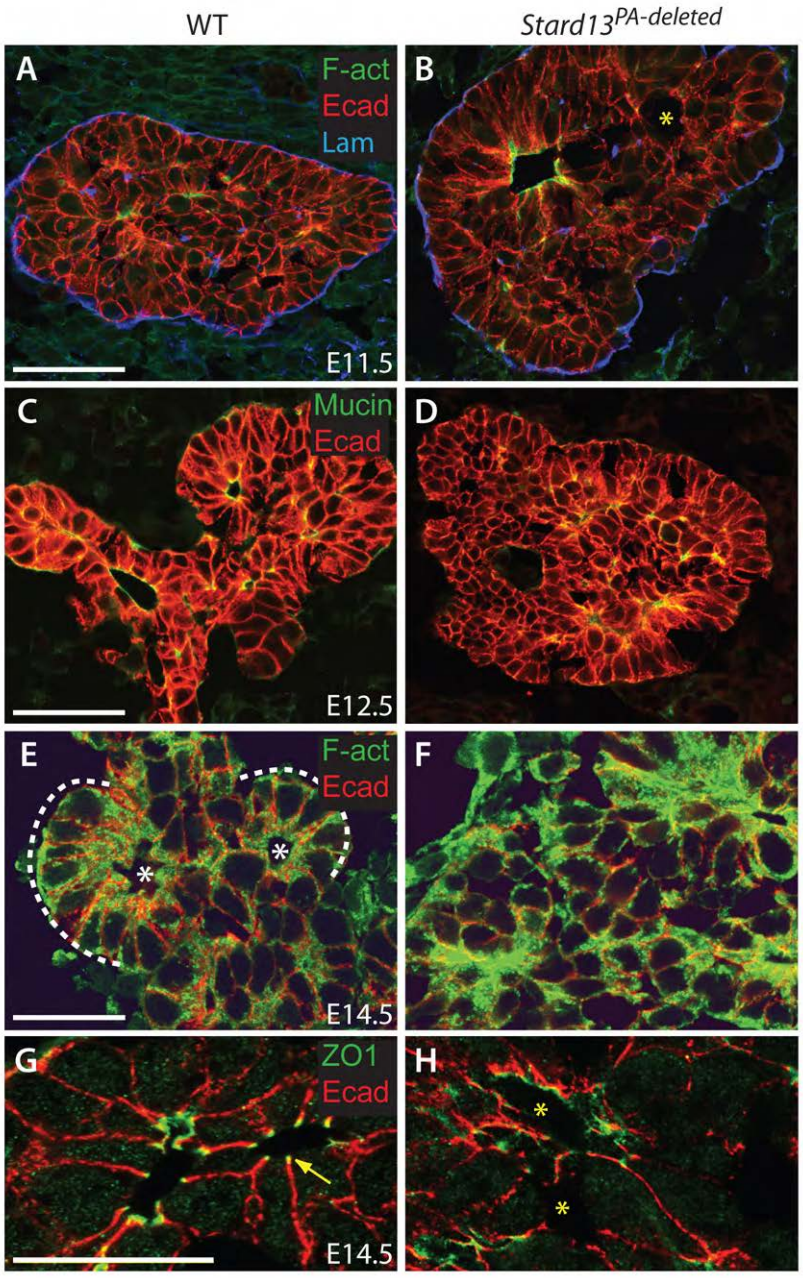


**Fig. S4. Distribution of epithelial polarity markers in the developing pancreas.** (**A**,**B**) WT and *Stard13*$^{PA\text{-}deleted}$ pancreatic sections were analysed for epithelial cell organisation with immunostaining for laminin (Lam), F-actin (F-act) and Ecad at E11.5. Microlumens were detected within the WT pancreatic epithelium and F-actin staining was properly distributed at the apical surface of the cells lining the lumens (A). In E11.5 *Stard13*$^{PA\text{-}deleted}$ pancreas, microlumens were not detected. By contrast, larger inner cavities surrounded by non-polarised cells with continuous E-cadherin membrane staining were found (B; asterisk). (**C**,**D**) Immunostaining for Mucin and Ecad at E12.5. *Stard13*$^{PA\text{-}deleted}$ cells display stratified and compact epithelial organisation with rare microlumens (D). (**E**,**F**) Immunostaining for F-act and Ecad at E14.5. *Stard13*$^{PA\text{-}deleted}$ cells display abnormal accumulation of F-actin (F). White outlines and asterisks indicate branches and lumens at E14.5, respectively (E). In the WT pancreas, F-actin filament meshwork normally underlay the apical pole, displaying a ratio of apical to basal mean fluorescence intensity between 1.5-1.6 A.U. on average, as measured by Image J. By contrast, in the absence of *Stard13* the measurable accumulation of F-actin at the basal pole is higher than in the control, resulting into a lower ratio of apical to basal mean fluorescence intensity (1.3-1.4 AU). This result suggests not only accumulation but also mislocalisation of the F-actin filaments in the absence of *Stard13*. (**G**,**H**) In E14.5 WT pancreatic epithelium, ZO-1 expression was detected at the apical edge of the junctional complex (arrow). In *Stard13*$^{PA\text{-}deleted}$ pancreas, newly forming lumens surrounded by either polarised or non-polarised cells were present (H). Asterisks indicate cavity surrounded by non-polarised cells. Scale bars: 50 μm (A-F); 20 μm (G,H).

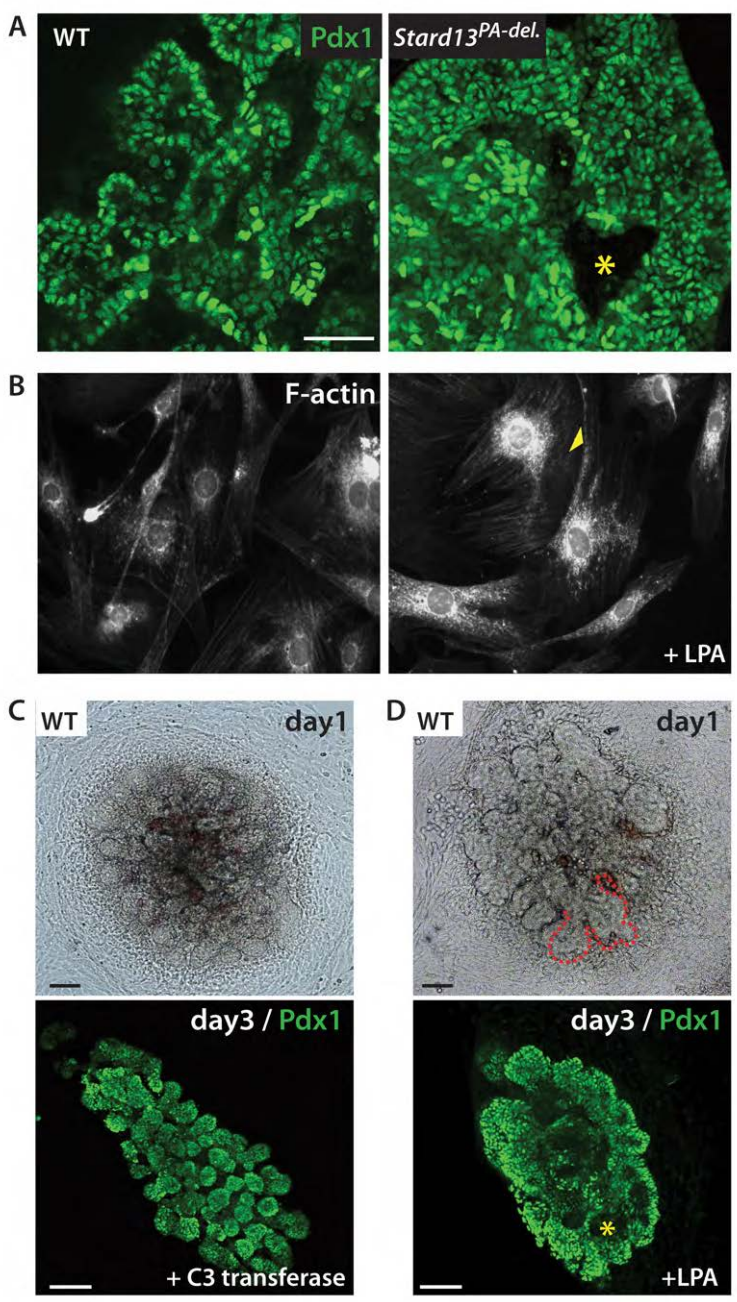


**Fig. S5. Pharmacological activation or inhibition of the Rho signaling.** (**A**) Whole-mount immunostaining for Pdx1 on WT explants showed tubules of Pdx1+ cells undergoing extensive branching by 48 hours of cultures. In *Stard13*$^{PA\text{-}deleted}$, pancreatic cells expressed Pdx1, but lacked tubules and typical branching organisation, as *in vivo*. Asterisk indicates internal cavity. (**B**) Activity of the LPA bioactive phospholipid was tested in embryonic fibroblast cultures using standard assays, such as staining of F-actin cytoskeleton with Alexa 488-phalloidin. Quiescent serum-starved mouse embryonic fibroblasts showed F-actin+ stress fibres. LPA treatment promoted flattening and increase in stress-fibre density (see yellow arrowhead), as result of RhoA activation. (**C**) Rho GTPase activity was selectively blocked through the use of a membrane-permeable version of the enzyme C3 transferase. E11.5 WT dorsal pancreases were cultured alone for 24 hours (day 1) and, subsequently, exposed to the C3 transferase during 48 hours. After 4 days, explants were fixed and immunostained with anti-Pdx1. C3 treatment did not perturb normal tubules formation and branching in WT developing pancreas. (**D**) In Rho activation assay, LPA was added at the final concentration of 10 μg/ml to the culture medium on day 1 and replaced every 24 hours. LPA-mediated activation of Rho reduced cell growth and antagonised tubulogenesis and branching in WT pancreatic epithelium, without affecting Pdx1 expression. Red outline indicates initiation of branching in WT pancreas organ culture after 24 hours in culture. Asterisk indicates internal cavities in LPA-treated explants. Scale bars: 50 μm (A); 100 μm (C,D).

## Table S1. Primer sequences

### Genotyping primers

| Gene | Primer | Sequence | Size (bp) |
|---|---|---|---|
| WT Stard13 | WT-fw | CAG TTC CAT GTT GGG TCT TCG T | 259 |
| | WT-rev. | CCT TCC AGC TGG GGG GTA GG | |
| Floxed Stard13 allele | Lox-fw | CAG TTC CAT GTT GGG TCT TCG T | 330 |
| | Lox-rev. | CCA GCT GGC TAG CTG GCA AAC | |
| Post-recombination product | Rec-fw. | CAG TTC CAT GTT GGG TCT TCG T | 700 |
| | Rec-rev. | AAC ATA CCT TAG ATC TAT TG | |
| Pdx1 Cre | Pdx1Cre-fw | tGC CAC GAC CAA GTG ACA GC | 600 |
| | Pdx1Cre-rev. | CCA GGT TAC GGA TAT AGT TCA TG | |

### RT-qPCR primers

| Gene | Accession number | Primer | Sequence | Size (bp) |
|---|---|---|---|---|
| 36B4 | NM_007475.5 | F | GGCCCTGCACTCTCGCTTTC | 124 |
| | | R | TGCCAGGACGCGCTTGT | |
| SDHA | NM_023281.1 | F | TGT TCA GTT CCA CCC CAC A | 100 |
| | | R | TCT CCA CGA CAC CCT TCT GT | |
| Srf | NM_020493.2 | F | GGCCGCGTGAAGATCAAGAT | 159 |
| | | R | CACATGGCCTGTCTCACTGG | |
| Ctgf | NM_010217.2 | F | CCCTAGCTGCCTACCGACT | 113 |
| | | R | CATTCCACAGGTCTTAGAACAG G | |
| Vcl | NM_009502.4 | F | GCAACCTCGTCCGGGTTGGAA | 163 |
| | | R | TCCCGCGCAGGAACCGAGTA | |
| Mig6 | NM_133753.1 | F | TGGCCTACAATCTGAACTCCC | 102 |
| | | R | GACCACACTCTGCAAAGAAGT | |
| β1-integrin | NM_010578.2 | F | GGCGGACGCTGCGAAAAGATG A | 160 |
| | | R | CCACCCACAATTTGGCCCTGCT | |
| α6-integrin | NM_008397.3 | F | CGGTCTCCGGAGTCGCTAAGC | 163 |
| | | R | TCAAGGTTGCTGTGCCGAGGTT | |

**Table S2. List of primary antibodies**

| Antibody | Raised in | Dilution | Source |
|---|---|---|---|
| Amylase | Rabbit | 1:500 | Sigma |
| Akt | Rabbit | 1:1000 | Cell Signaling |
| pAkt | Rabbit | 1:1000 | Cell Signaling |
| F-actin | FITC-conj. | 1:500-1:750 | Molecular Probes |
| Carboxypeptidase 1 | Rabbit | 1:500 | AbD Serotec |
| E-cadherin | Rat | 1:500-1:1000 | Invitrogen |
| ERK1/2 | Rabbit | 1:1000 | Cell Signaling |
| pERK1/2 | Rabbit | 1:1000 | Cell Signaling |
| GAPDH | Rabbit | 1:1000 | Cell Signaling |
| Glucagon | Rabbit | 1:500 | Immunostar |
| GST | Rabbit | 1:100 | Santa Cruz |
| Phospho-Histone H3 (Er10) | Rabbit | 1:200 | Millipore |
| Insulin | Guinea pig | 1:250 | Millipore |
| Laminin | Rabbit | 1:1000 | Sigma |
| Mig6 | Rabbit | 1:100 | Santa Cruz |
| Mucin | Armenian hamster | 1:1000 | Thermo Scientific |
| Phospho-MLC2 | Rabbit | 1:200 | Cell Signaling |
| Neurogenin 3 | Guinea pig | 1:2000 | Gift of M. Sander, UCSD, San Diego, CA, USA |
| Pdx1 | Rabbit | 1:2000 | Abcam |
| Pdx1 | Mouse | 1:100 | Hybridoma Bank |
| PKCζ | Rabbit | 1:100 | Santa Cruz |
| Ptf1a | Rabbit | 1:2500 | Gift of A. Sprinkler, BCBC Antibody Core, Novo Nordisk, Denmark |
| Sox-9 | Rabbit | 1:2000 | Gift of M. Wegner, Erlangen University, Germany |
| YAP | Rabbit | 1:100 | Cell Signaling |
| p-YAP | Rabbit | 1:100 | Cell Signaling |
| ZO-1 | Rabbit | 1:100 | Invitrogen |